SAND REPORT
SAND2002-4179
Unlimited Release
Printed March 2003

CFD Modeling of Natural Convection Heat Transfer and Fluid Flow in Yucca Mountain Project (YMP) Enclosures

Nicholas D. Francis, Jr., Stephen W. Webb, Michael T. Itamura, and Darryl L. James

Prepared by
Sandia National Laboratories
Albuquerque, New Mexico 87185 and Livermore, California 94550

Sandia is a multiprogram laboratory operated by Sandia Corporation, a Lockheed Martin Company, for the United States Department of Energy under Contract DE-AC04-94AL85000.

Approved for public release; further dissemination unlimited.

Issued by Sandia National Laboratories, operated for the United States Department of Energy by Sandia Corporation.

NOTICE: This report was prepared as an account of work sponsored by an agency of the United States Government. Neither the United States Government, nor any agency thereof, nor any of their employees, nor any of their contractors, subcontractors, or their employees, make any warranty, express or implied, or assume any legal liability or responsibility for the accuracy, completeness, or usefulness of any information, apparatus, product, or process disclosed, or represent that its use would not infringe privately owned rights. Reference herein to any specific commercial product, process, or service by trade name, trademark, manufacturer, or otherwise, does not necessarily constitute or imply its endorsement, recommendation, or favoring by the United States Government, any agency thereof, or any of their contractors or subcontractors. The views and opinions expressed herein do not necessarily state or reflect those of the United States Government, any agency thereof, or any of their contractors.

Printed in the United States of America. This report has been reproduced directly from the best available copy.

Available to DOE and DOE contractors from
U.S. Department of Energy
Office of Scientific and Technical Information
P.O. Box 62
Oak Ridge, TN 37831

Telephone: (865)576-8401
Facsimile: (865)576-5728
E-Mail: reports@adonis.osti.gov
Online ordering: http://www.doe.gov/bridge

Available to the public from
U.S. Department of Commerce
National Technical Information Service
5285 Port Royal Rd
Springfield, VA 22161

Telephone: (800)553-6847
Facsimile: (703)605-6900
E-Mail: orders@ntis.fedworld.gov
Online order: http://www.ntis.gov/help/ordermethods.asp?loc=7-4-0#online

SAND2002-4179
Unlimited Release
Printed March 2003

CFD Modeling of Natural Convection Heat Transfer and Fluid Flow in Yucca Mountain Project (YMP) Enclosures

Nicholas D. Francis, Jr., and Michael T. Itamura
Subsystems Performance Assessment Department

Stephen W. Webb
Environmental Technology Department

Sandia National Laboratories
P.O. Box 5800
Albuquerque, NM 87185-0776

Darryl L. James
Texas Tech University
Department of Mechanical Engineering
Box 41021
Lubbock, TX 79409-1021

ABSTRACT

For the Yucca Mountain Project (YMP), cooling of spent nuclear waste emplaced in tunnels bored into volcanic tuff is important to the performance of the proposed nuclear waste repository. The geometry consists of an emplacement drift (tunnel), waste package, and a layer of gravel invert at the bottom of the drift. In some cases, a drip shield, which is a thin metal sheet that covers the waste package, is also included. The YMP geometry is in essence an annulus where the inner cylinder represents the waste package and the outer cylinder represents the emplacement drift. The waste package is below the centerline of the drift, so the geometry is eccentric. The invert forms a flow blockage in the lower portion of the annulus. In the cases with a drip shield, an additional flow barrier is present. Both repository periods (pre- and post-closure) contain a natural convection component. During pre-closure, mixed convection is important due to ventilation and natural convection in combination. During post closure, natural convection is the only mode of fluid flow due to the lack of ventilation.

The objective of this report is to develop two-dimensional computational fluid dynamics (CFD) numerical simulations based on YMP geometries (25%, 44%, and full-scale) and compare the steady-state heat transfer results from these simulations to natural convection heat transfer correlation equations in the literature. A number of different heat transfer expressions have been developed in the literature to compute average equivalent thermal conductivities. However, these expressions have primarily been developed for horizontal concentric cylinder arrangements of very

small inner and outer radii and gap-widths. In this comparative study, interest is primarily focused on the YMP geometry with eccentric placement and a flow blockage for annuli of large gap width and radius ratio.

CFD predicted heat transfer rates from YMP geometries without drip shields are from 1/3 to 1/2 less than concentric annulus heat transfer rates quoted in the literature. Likewise, for models including drip shields, the literature correlation equations overestimate heat transfer rates both inside and outside the drip shield. Therefore, new heat transfer correlation equations are developed specifically for YMP using CFD results. Average equivalent thermal conductivity relationships for the full-scale geometry (both with and without a drip shield) are developed in terms of temperature difference and characteristic gap-width.

CONTENTS

FIGURES

Page

TABLES

Page

NOMENCLATURE

A_c	cross-sectional area (m^2)
A_i	component surface area on the inside surface of an enclosure (m^2)
A_o	component surface area on the outside surface of an enclosure (m^2)
c_p	fluid specific heat (J/kg-K)
D_i	inner cylinder diameter (m)
D_o	outer cylinder diameter (m)
g	acceleration due to gravity (m/s^2)
k_a	stagnant air thermal conductivity (W/m-K)
k_{eq}	average equivalent thermal conductivity for natural convection (-), $k_{eff,th}/k_a$
k_{eq_j}	local equivalent thermal conductivity for natural convection (-)
$k_{eff,th}$	effective thermal conductivity including the effects of the natural convection (W/m-K)
L	gap-width (m), $R_o - R_i$
L_c	characteristic gap-width (m)
M_w	molecular weight of air (kg/kmol)
P	wetted perimeter (m)
Pr	Prandtl number (-)
Q	overall heat transfer rate from the CFD models (W)
Q_{cond}	conduction heat transfer rate from the CFD models (W)
q_i	component heat flux on the inside surface of an enclosure (W/m^2)
q_o	component heat flux on the outside surface of an enclosure (W/m^2)
q_{cond_i}	component conduction heat flux on the inside surface of an enclosure (W/m^2)
q_{cond_o}	component conduction heat flux on the outside surface of an enclosure (W/m^2)
R_g	universal gas constant (N-m/kmol-K)
Ra_L	Rayleigh number based on gap-width (-)
Ra_{L_c}	Rayleigh number based on characteristic gap-width (-)
R_o	outside radius (m)
R_i	inside radius (m)
T_c	cold cylinder (outer) wall temperature (K or ^oC)
T_h	hot cylinder (inner) wall temperature (K or ^oC)
T_m	middle temperature (K or ^oC)
ΔT	temperature difference, $T_h - T_c$, $T_h - T_m$, or $T_m - T_c$ (^oC)

Greek

α	fluid thermal diffusivity (m^2/s)
β	volumetric thermal expansion coefficient ($=1/T$) (K^{-1})
ε	eccentricity (m)
θ	angular position (0^o is vertical up, 180^o is vertical down)
ν	fluid kinematic viscosity (m^2/s)
ρ	fluid density (kg/m^3)

ACKNOWLEDGEMENTS

The authors would like to thank Charles E. Hickox, Jr., of Sandia National Laboratories and Veraun Chipman of Lawrence Livermore National Laboratory for their thorough reviews of this document. This work was supported by the Yucca Mountain Office of Repository Development as part of the Office of Civilian Radioactive Waste Management (OCRWM), which is managed by the U.S. Department of Energy, Yucca Mountain Office of Repository Development. Sandia is a multiprogram laboratory operated by Sandia Corporation, a Lockheed Martin Company, for the United States Department of Energy under Contract DE-AC04-94AL85000.

Intentionally Left Blank

1 INTRODUCTION

This report documents a comparison of computational fluid dynamics (CFD) simulations of natural convection in the annulus formed by the YMP geometric layout with experimental data in the heat transfer literature. The YMP annulus is characterized by an inner cylinder (waste package) eccentrically placed within the outer cylinder (emplacement drift). A flow blockage (invert layer) exists below the inner cylinder. In some cases, the inner cylinder is surrounded by a drip shield. Refer to Figure 1 for a schematic of the modeled geometry. Proposed repository operation occurs in two periods. The ventilated repository pre-closure period is characterized by mixed convection (e.g., both forced and natural convection play a role in the heat transfer). No drip shield is emplaced during the pre-closure period. Because pre-closure does indeed possess a natural convection component, the analysis described in this report provides a correlation equation specific to YMP for the natural convection component. The repository post-closure period is characterized by no ventilation and drip shield emplacement. The analysis described in this report provides correlation equations inside and outside the drip shield during post-closure.

CFD simulations are used to compute overall heat transfer rates specific to the YMP geometry. The calculated heat transfer rates are compared to the correlation equations developed by Kuehn and Goldstein (1976b, 1978) for horizontal concentric cylinders. In this comparative study, interest is primarily focused on large gap widths (on the order of 0.5 m or greater) and radius ratios ($R_o/R_i \approx$ 3.2-3.5). Additionally, the influence of a complex geometry on overall heat transfer characteristics is included. The heat transfer results derived in this report have been correlated specifically for the YMP geometry. A previous CFD analysis of natural convection heat transfer detailed a comparison between the literature and CFD simulations using YMP-geometric scales applied to horizontal concentric cylinder arrangements (Francis et al., 2002). That analysis showed good model to data comparison at both laminar and turbulent Rayleigh numbers.

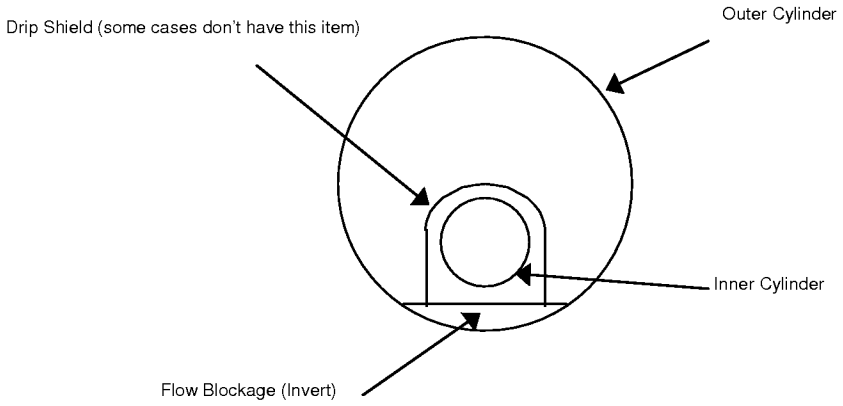

Figure 1. Schematic of the Modeled Geometry.

The CFD code, FLUENT, version 6.0.12 (Fluent Incorporated, 2001), is used for the analysis. FLUENT is a computational fluid dynamics code that solves conservation of mass, momentum, energy (including radiative transfer equations), species, and turbulence models using various means to obtain closure for the turbulent momentum equations. Transient or steady state formulations are available. For this heat transfer analysis, both steady-state laminar and turbulent natural convection heat transfer are considered.

2 MODEL DESCRIPTION AND COMPARISON TO LITERATURE RESULTS

This section provides a brief discussion of previous natural convection heat transfer experiments, correlation equations, and numerical simulations. Also, reference should be made to Francis et al., 2002, for additional information related to this topic. In the literature, a variety of heat transfer correlation equations have been developed for internal natural convection heat transfer in horizontal concentric cylinders. However, the equations are typically based on experimental results from very small inner and outer cylinder radii (on the order of a few centimeters) and gap-widths (1.9 cm $\leq L \leq$ 7.1 cm). In this report, literature correlation equations are applied to much larger gap-widths (0.5 m $\leq L \leq$ 1.9 m) and cylinder radii (0.2 m $\leq R_i$, $R_o \leq$ 2.75 m). Although the Yucca Mountain Project (YMP) geometries are not concentric (refer to Figure 1), a typical simplifying assumption is often made such that an equivalent thermal conductivity for natural convection can be computed with an existing (literature) correlation applied at a geometric scale appropriate to YMP. The resulting equivalent thermal conductivity is then applied to a non-concentric annulus. This analysis provides an assessment of the applicability of existing heat transfer correlations to the YMP geometries.

2.1 Introduction

Previous experimental and theoretical studies of internal natural convection in the annulus between horizontal cylinders have been largely restricted to simple geometries such as concentric or eccentric horizontal cylinders. In many of these cases, the geometries have small (~ 3 cm) gap widths ($L = R_o - R_i$). Typically, a single radius ratio was considered (e.g., Kuehn and Goldstein, 1976, considered a radius ratio of 2.6; Bishop, 1988, and McLeod and Bishop, 1989, considered a radius ratio of 3.37; Vafai et al., 1997, considered a radius ratio of 1.1). A limited number of numerical and experimental studies have investigated the influence of the radius ratio on internal flow characteristics (Lis, 1966; Bishop et al, 1968; Desai and Vafai, 1994; Char and Hsu, 1998). Some investigators developed heat transfer correlation equations for their experimental results (Lis, 1966; Bishop et al, 1968; Kuehn and Goldstein, 1976a; Kuehn and Goldstein, 1978; Bishop, 1988). In the experimental studies, a range of radius ratios considered was $1.1 \leq R_o/R_i \leq 4$. In the numerical studies, a wider range of radius ratios was considered ($1.5 \leq R_o/R_i \leq 11$), including a radius ratio of 3.5, which is similar to that of the YMP geometry (Webb et al., 2002). In the present comparative study, interest is focused on large gap widths (on the order of 0.5 m or greater) and radius ratios ($R_o/R_i \approx$ 3.2-3.5). Additionally, this report investigates the influence of geometry (e.g., gap width, flow blockage) on local and overall heat transfer characteristics.

Most of the concentric and eccentric geometric modeling studies consider gases (Pr ≈ 0.7) as the working fluid in the annulus (Kuehn and Goldstein, 1976a; Kuehn and Goldstein, 1978; Farouk and Guceri, 1982; Desai and Vafai, 1994); although, some investigated a larger range of Prandtl numbers (Kuehn and Goldstein, 1976a; Desai and Vafai, 1994). A number of experimental analyses considered water (Pr ≈ 5) as the working fluid in the annulus (Kuehn and Goldstein, 1976a). Some numerical studies considered Prandtl numbers as high as 5000 (engine oil at room temperature) and as low as about 0.01 (liquid metals). The present study only considers gases with a Prandtl number of approximately 0.7 (e.g., air, nitrogen).

Table 1 lists the investigators and the forms in which their natural convection heat transfer investigations were presented (experiment, correlation equation, and numerical simulations).

Table 1. Internal Natural Convection Heat Transfer in the Literature

Investigators	Experimental Data	Correlation Equation	Numerical Simulation
Bishop, 1988	X	X	
Bishop et al., 1968	X	X	
Char and Hsu, 1998			X
Desai and Vafai, 1994			X
Farouk and Guceri, 1982			X
Fusegi and Farouk, 1986			X
Francis et al., 2002			X
Kuehn, 1976	X	X	X
Kuehn and Goldstein, 1976a	X	X	X
Kuehn and Goldstein, 1976b		X	
Kuehn and Goldstein, 1978	X	X	
J. Lis, 1966	X	X	
McLeod and Bishop, 1989	X	X	
Raithby and Hollands, 1975		X	X
Vafai et al., 1997	X	X	X
Webb et al., 2002	X		X

For internal natural convection in an annulus, a Rayleigh number based on gap-width

$$Ra_{L_c} = \frac{g\beta\Delta T L_c^{\,3}}{\nu\alpha} \tag{1}$$

is normally used to determine if the internal flow is laminar or turbulent (Kuehn and Goldstein, 1978). The Rayleigh number in equation (1) is based on a characteristic gap-width given by the following relationship:

$$L_c = \frac{2A_c}{P} \tag{2}$$

where A_c is the cross-sectional area of the flow domain and P is the wetted perimeter of the bounding walls. It is noted that equation (2) reduces to the standard gap-width definition, $L = R_o - R_i$, for a

horizontal concentric cylinder annulus.

The transition gap-width Rayleigh number for turbulence is about 10^6 (Kuehn and Goldstein, 1978; Desai and Vafai, 1994; Char and Hsu, 1998). For Rayleigh numbers less than 10^6, the flow is laminar. For Rayleigh numbers greater than this transition value, the horizontal annulus internal flow conditions for a heated inner cylinder are characterized by a turbulent upward moving plume above the inner heated cylinder and a turbulent downward flow against the cooled outer wall. Stagnation regions exist near the top where the plume impinges on the outer cylinder and over the entire bottom of the annulus. A low velocity core region exists in the annulus away from the walls. The two-dimensional CFD models discussed in this report are applied at both laminar and turbulent flow Rayleigh numbers. The turbulent flow conditions are modeled using the RNG k-ε turbulence model as described in detail in Francis et al., (2002), for horizontal concentric cylinders of various sizes.

Turbulent flow conditions in the annulus are typically obtained either through the length scale (e.g., gap width) or the operating conditions (e.g., temperature difference and operating pressure) of the configuration. For the very small gap widths (~ 3 cm) considered in the experiments presented in the literature, air at atmospheric temperatures and pressures would not result in fully turbulent Rayleigh numbers (e.g., $Ra_L < 10^6$). Pressurized gases such as nitrogen were often used in experiments to obtain the fluid properties necessary to achieve turbulent Rayleigh numbers for very small gap widths and small temperature differences (Kuehn and Goldstein, 1978). The results of the experiments were then used to establish correlation equations that relate fluid properties and apparatus geometry to average heat transfer rates. Numerical models have been developed for some of the experimental geometries to compare model predictions to measured temperatures and heat transfer coefficients. Most of the numerical models are two-dimensional, but a limited number of three-dimensional studies have been conducted (Fusegi and Farouk, 1986; Desai and Vafai, 1994).

The CFD model comparison to Kuehn and Goldstein's (1976b and 1978) average heat transfer correlations is selected in this report because these correlations are widely considered standards in the natural convection heat transfer literature. Other correlation and data results are presented in Francis et al., 2002.

Most of the experimental data discussed above and presented in the literature are restricted to heat transfer results such as temperature and equivalent thermal conductivity. Experimental measurements of fluid velocity and turbulence quantities have not been published in the literature for the horizontal concentric cylinder geometry.

2.2 Grid Specifications for YMP Geometries

The YMP geometry consists of an emplacement drift (outer cylinder), waste package (inner cylinder), and a layer of gravel invert at the bottom of the drift. In some cases, a drip shield, which is a thin metal sheet that covers the waste package, is also included. This geometry is essentially an annulus where an inner cylinder represents the waste package and an outer cylinder represents the emplacement drift wall. The waste package is below the centerline of the drift, so the geometry is eccentric. The invert floor forms a flow blockage in the lower portion of the annulus. In the cases

with a drip shield, an additional flow barrier that surrounds the inner cylinder is present. Refer to Figure 1 for an illustration of the modeled geometry.

2.2.1 Without Drip Shield

The geometric specifications for the numerical simulations without a drip shield are given in Table 2 for three YMP scales (25%, 44%, full-scale). The 25% and 44%-scale geometries represent scaled natural convection experiments conducted at the Atlas facility in Las Vegas, Nevada. The CFD modeling of those tests is described in Francis et al., 2003. Three different inner cylinder diameters, including a minimum, average, and maximum, are considered for the full-scale geometry as indicated in Table 2. The inner cylinder is translated a given distance (ε) below the centerline position of the outer cylinder. Additionally, an invert layer is specified below the inner cylinder. The invert layer serves as a flow blockage with respect to the outer cylinder (refer to the schematic shown in Figure 1 and the computational grid shown in Figure 2). Simply put, the invert is a floor below the heated inner cylinder.

Table 2. Approximate YMP Geometries without Drip Shield

Case	Inner Cylinder D_i (m)	Outer Cylinder D_o (m)	Eccentricity ε (m)	D_o/D_i	Flow Blockage (Invert) Height (m)	L_c (m)
25%-Scale YMP	0.4	1.37	0.2	3.4	0.2	0.45
44%-Scale YMP	0.7	2.42	0.4	3.5	0.35	0.79
Full-Scale YMP	1.7[a]	5.5	0.8	3.2	0.8	1.74
Full-Scale YMP	1.24	5.5	0.9	4.4	0.8	1.97
Full-Scale YMP	2	5.5	0.7	2.7	0.8	1.58

a – approximate average inner cylinder diameter

The table includes the modeled case, inner and outer cylinder diameters, diameter ratio, approximate eccentricity and invert height, and a characteristic gap-width obtained from equation (2). Eccentricities and invert heights given in the table are based on a full-scale invert height of 0.8 meters and a clearance of the inner cylinder above the invert floor of between 0.24 and 0.41 meters.

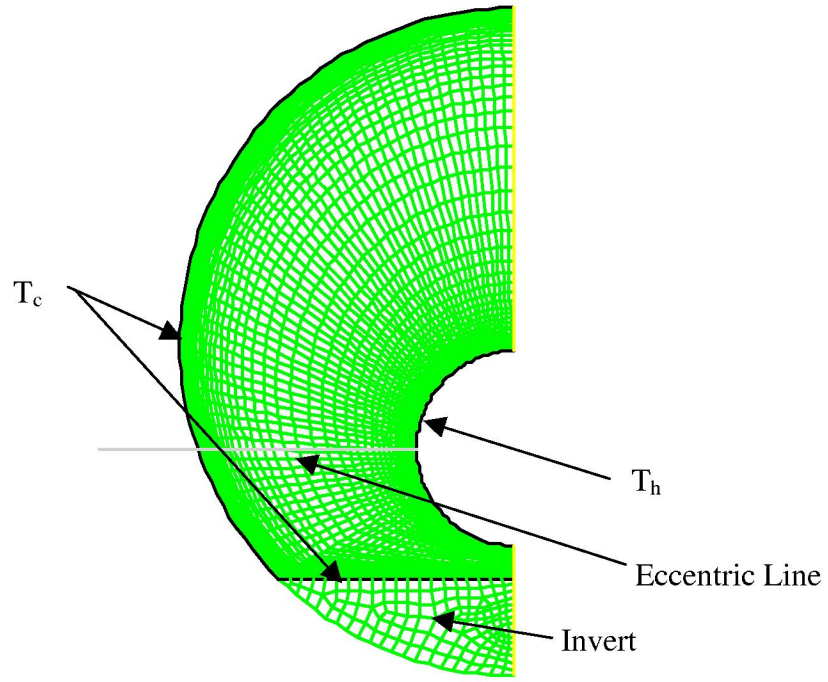

Figure 2. Computational Grid for the 25%-Scale YMP Geometry.

The radial and angular discretization for the geometries without a drip shield (25%-scale, 44%-scale, and full-scale) is described below. The computational grid for the 25%-scale numerical simulation is shown in Figure 2. The other grids are similar. In the case of the 25%-scale, 44%-scale, and full-scale geometries, the radial discretization includes 61 intervals. Each geometry requires cell clustering at the inner and outer walls to resolve the boundary layers that form there. The cell-clustering factor for the two larger geometries is 1.2 towards both walls. The cell-clustering factor for the 25%-scale geometry is 1.15 towards both walls (shown in Figure 2). Because the Rayleigh number is lower for the 25%-scale case, fewer cells are required adjacent to the walls.

Angular discretization for the full-scale, 44%-scale, and 25%-scale YMP geometries is 77, 86, and 81, respectively. A slight cell clustering is applied in the angular direction of the full-scale geometry near the buoyant plume that develops between cylinders.

2.2.2 With Drip Shield

The YMP geometries with a drip shield are similar to those without a drip shield. For the drip shield cases, a characteristic gap-width based on equation (2) is computed both inside and outside the drip shield (see Table 3).

Table 3. Approximate YMP Geometries with Drip Shield

Case	Inner Cylinder D_i (m)	Outer Cylinder D_o (m)	Eccen ε (m)	D_o/D_i	Flow Blockage (Invert) Height (m)	L_c (m) (inside)	L_c (m) (outside)
25%-Scale YMP	0.4	1.37	0.2	3.4	0.2	0.14	0.37
44%-Scale YMP	0.7	2.42	0.4	3.5	0.35	0.21	0.69
Full-Scale YMP	1.7[a]	5.5	0.8	3.2	0.8	0.49	1.5
Full-Scale YMP	1.24	5.5	0.9	4.4	0.8	0.88	1.5
Full-Scale YMP	2	5.5	0.7	2.7	0.8	0.33	1.5

a – average inner cylinder diameter

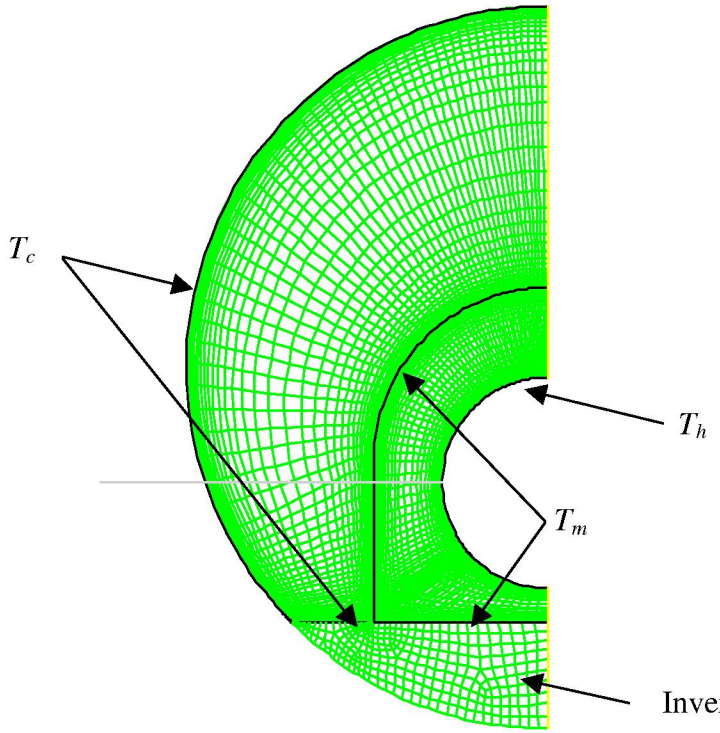

Figure 3. Computational Grid for the 25%-Scale YMP Geometry (with Drip Shield).

The radial and angular discretization for the geometries with a drip shield (25%-scale, 44%-scale, and full-scale) is described below. The computational grid for the 25%-scale numerical simulation is shown in Figure 3. The other grids are similar. The radial discretization outside the drip shield varies from 40 to 60 cells. The radial discretization inside the drip shield varies from 31 to 50 cells. Each geometry requires cell clustering in the radial direction at the walls to resolve the boundary layers. The angular discretization varies from 92 to 119 cells. Cell clustering occurs at the top of the annulus were the heated plume ascends and impinging flow turns downward and near the invert floor were flow turns upward.

2.3 Boundary Conditions

2.3.1 Without a Drip Shield

Constant temperature boundary conditions are applied to the geometries without drip shield. The temperature boundary conditions are specified to give a temperature difference (ΔT) across the inner and outer cylinders that is comparable to that expected between the waste package and the drift wall at the proposed Yucca Mountain repository. The hot temperature (T_h) of the inner cylinder is assumed to be 373K and the cold temperature (T_c) of the outer cylinder and invert is assumed to be 353K, which results in a ΔT of 20°C. The numerical simulations for all three geometric scales apply a 20°C temperature difference at the boundaries. Additionally, the full-scale YMP geometry is also evaluated at temperature differences of 5 and 50°C. For a temperature difference of 5°C, the constant boundary temperatures are 365.5K and 360.5K. For a temperature difference of 50°C, the constant boundary temperatures are 388K and 338K. Refer to Figure 2 for identification of the constant temperature boundaries.

- $\Delta T = 5$°C; $T_h = 365.5$K, $T_c = 360.5$K
- $\Delta T = 20$°C; $T_h = 373$K, $T_c = 353$K
- $\Delta T = 50$°C; $T_h = 388$K, $T_c = 338$K

The average fluid temperature is identical (363K) for each ΔT. The temperature difference is more important than the actual temperatures (although properties vary slightly with temperature) in the natural convection calculations because it, along with the geometry, determines the Rayleigh number. For the YMP geometries, the top of invert is also specified at a temperature of T_c (see Figure 2) in order to ascertain the effect of the YMP geometry on overall heat transfer, and subsequently, the average equivalent thermal conductivity.

2.3.2 With a Drip Shield

Constant temperature boundary conditions are applied to the geometries with a drip shield. The inner cylinder is maintained at a constant temperature, T_h. The drip shield and inner invert surface under the drip shield are specified at a constant temperature, T_m. The outer cylinder surface and outer invert surface are maintained at a constant temperature, T_c. The numerical simulations for all three geometric scales apply the same 20°C overall temperature difference. Additionally, the full-scale YMP geometry is also evaluated at overall temperature differences of 5 and 50°C. The overall temperature difference is defined between T_h and T_c. The overall temperature difference is segregated by T_m.

The temperature differences $T_h - T_m$ and $T_m - T_c$ are based on the results of an analyses described in Francis et. al., 2003a. Ultimately, the selection of a temperature difference (e.g., $T_m - T_c$) is somewhat arbitrary in this analysis. The primary goal of this report is to establish a reasonable range of potential temperature differences so that the ensuing heat transfer correlation equations developed for YMP specific geometries can be applied over a broad range of temperature conditions.

Constant temperature boundaries are specified such that the fluid space inside the drip shield is

always maintained at the same average temperature (367.6K) for any ΔT. The average fluid temperature outside the drip shield is not maintained constant. For an overall temperature difference of 20°C, $T_h - T_m$ and $T_m - T_c$ are 10.8 and 9.2, respectively. For an overall temperature difference of 5°C, $T_h - T_m$ and $T_m - T_c$ are 2.7 and 2.3, respectively. Finally, for an overall temperature difference of 50°C, $T_h - T_m$ and $T_m - T_c$ are 27 and 23, respectively. The constant temperature boundary conditions applied in the CFD simulations are given below and illustrated in Figure 3.

- $\Delta T = 5$°C; $T_h = 368.95$K, $T_m = 366.25$K, $T_c = 363.95$K
- $\Delta T = 20$°C; $T_h = 373$K, $T_m = 362.2$K, $T_c = 353$K
- $\Delta T = 50$°C; $T_h = 381.1$K, $T_m = 354.1$K, $T_c = 331.1$K

2.3.3 All Geometries

A vertical plane through the geometric center forms a symmetry boundary (half domain modeled due to symmetry) as illustrated earlier in Figures 2 and 3. The existence of a steady-state solution is tacitly assumed since symmetry boundary conditions are imposed on the numerical simulations. Steady laminar flow has been found experimentally for low Rayleigh numbers (Kuehn and Goldstein 1976a). At Rayleigh numbers of the order of 10^7, the wall boundary layers are steady (Kuehn and Goldstein 1978). For larger Rayleigh numbers ($> 10^8$), it is assumed that a steady-state solution is achievable because the solutions converged. However, it is possible that some flow regimes (presumably at high Rayleigh numbers) may not exhibit steady-state behavior. This possibility will be investigated in future CFD analyses.

2.4 Thermal Properties

Thermophysical properties of dry air are applied in the CFD simulations. The properties are evaluated at the average fluid temperatures given in Table 4.

Table 4. Thermophysical Properties of Air[1]

Property	363K (No drip shield), all ΔT	367.6K (Inside drip shield), all ΔT	365.1K (Outside drip shield), ΔT = 5°C	357.6K (Outside drip shield), ΔT = 20°C	342.6K (Outside drip shield), ΔT = 50°C
Density,[2] ρ (kg/m^3)	0.97	0.96	0.97	0.99	1.03
Specific heat, c_p (J/kg-K)	1010.25	1010.58	1010.40	1009.83	1008.71
Thermal conductivity, k_a (W/m-K)	0.031	0.0314	0.0312	0.0304	0.0289
Dynamic viscosity, μ (kg/m-s)	2.135×10^{-5}	2.155×10^{-5}	2.144×10^{-5}	2.11×10^{-5}	2.043×10^{-5}
Kinematic viscosity, ν (m^2/s)	2.19×10^{-5}	2.24×10^{-5}	2.21×10^{-5}	2.13×10^{-5}	1.98×10^{-5}
Thermal diffusivity, α (m^2/s)	3.15×10^{-5}	3.23×10^{-5}	3.19×10^{-5}	3.04×10^{-5}	2.77×10^{-5}
Volumetric thermal expansion coefficient, β (K^{-1})	2.75×10^{-3}	2.72×10^{-3}	2.74×10^{-3}	2.8×10^{-3}	2.92×10^{-3}
$g\beta/\nu\alpha$ (m^{-3}*K^{-1})	4.05×10^{7}	3.79×10^{7}	3.93×10^{7}	4.35×10^{7}	5.18×10^{7}

1 - Bejan 1995, Appendix D
2 – used to compute Rayleigh numbers given in Table 5

2.4.1 Incompressible ideal gas

For all simulations in this report, the dynamic viscosity, molecular thermal conductivity, and specific heat are inputs in the numerical simulations as specified in Table 4. Each thermal quantity except the fluid density is treated as a constant. The fluid density is computed by FLUENT using the incompressible-ideal-gas law. The incompressible-ideal-gas law is

$$\rho = \frac{P_o}{\frac{R_g}{M_w} T} \tag{3}$$

where P_o is the operating pressure described in the next section and T is the fluid temperature. The incompressible-ideal-gas law is used (by FLUENT) when pressure variations are small enough such

that the overall internal flow conditions are essentially incompressible, but a relationship between density and temperature is required because this is the driving force for flow (buoyancy), which is the case for natural convection.

2.5 Operating Conditions

The operating pressure selected for the numerical simulations is 101.3 kPa. Standard atmospheric pressure at sea level is selected to perform a comparison to literature heat transfer results for natural convection (both data and correlation equations). The specified initial gauge pressure is 0 Pa for each simulation. The absolute pressure is computed as the operating pressure plus the gage pressure, or 101.3 kPa in this case. Gravity is specified in each of the simulations as 9.81 m/s^2. It is noted that a wide range of Rayleigh numbers result from the temperature differences (ΔT = 5, 20, 50°C) and characteristic gap-widths (Tables 2 and 3) applied in this analysis. Additionally, the range of Rayleigh number applicability is further increased by scaling gravity as indicated in Table 5. To achieve lower Rayleigh numbers for a given geometry and temperature difference, the gravity vector is simply scaled below its nominal value. For instance, if for a given geometry and temperature difference, a gravity vector (-g) of 9.81 m/s^2 results in a Rayleigh number of $1x10^8$, a gravity vector of (9.81/10) m/s^2 results in a Rayleigh number of $1x10^7$ for the same temperature difference and length scale. Using characteristic gap-widths as the length scale in the Rayleigh numbers, the operating conditions for each YMP geometry are given in Table 5.

Table 5. Operating Conditions

Case	Gravity, -g (m/s^2)	ΔT (°C)	Eccentric with Invert Ra_{L_c}	Eccentric with Invert and Drip Shield (Inside) Ra_{L_c}	Eccentric with Invert and Drip Shield (Outside) Ra_{L_c}
25% Scale	0.0981	20	$6.9x10^5$	$1.07x10^4$	$2.02x10^5$
25% Scale	0.981	20	$6.9x10^6$	$1.07x10^5$	$2.02x10^6$
25% Scale	9.81	20	$6.9x10^7$	$1.07x10^6$	$2.02x10^7$
44% Scale	0.0981	20	$3.86x10^6$	$3.79x10^4$	$1.3x10^6$
44% Scale	0.981	20	$3.86x10^7$	$3.79x10^5$	$1.3x10^7$
44% Scale	9.81	20	$3.86x10^8$	$3.79x10^6$	$1.3x10^8$
Full Scale	0.00981	20	$4.11x10^6$	$4.54x10^4$	$1.32x10^6$
Full Scale	0.0981	20	$4.11x10^7$	$4.54x10^5$	$1.32x10^7$
Full Scale	0.981	20	$4.11x10^8$	$4.54x10^6$	$1.32x10^8$
Full Scale	4.905	20	$2.05x10^9$	-	-
Full Scale	9.81	20	$4.11x10^9$	$4.54x10^7$	$1.32x10^9$
Full Scale	9.81	5	$7.74x10^8$	$3.71x10^6$	$2.96x10^8$
Full Scale	9.81	5	$1.03x10^9$	$1.14x10^7$	$2.96x10^8$
Full Scale	9.81	5	$1.5x10^9$	$6.69x10^7$	$2.96x10^8$
Full Scale	9.81	20	$3.09x10^9$	$1.48x10^7$	$1.32x10^9$
Full Scale	9.81	20	$5.99x10^9$	$2.68x10^8$	$1.32x10^9$
Full Scale	9.81	50	$7.74x10^9$	$3.71x10^7$	$4.05x10^9$
Full Scale	9.81	50	$1.03x10^{10}$	$1.14x10^8$	$4.05x10^9$
Full Scale	9.81	50	$1.5x10^{10}$	$6.69x10^8$	$4.05x10^9$

- Simulation not performed

Based on Table 5 and an assumed transition Rayleigh number of 10^6, most of the flow conditions are turbulent for the gap-widths and temperature differences considered in this report. Therefore, a turbulence flow model is required when solving the governing conservation equations as described in Francis et al., 2002. For the lower Rayleigh number flows (some of the 25%-scale models in Table 5), laminar flow equations are solved.

2.6 CFD Model Settings and Parameters

The CFD model settings and runtime monitoring for equation residuals, discretization, convergence, and steady-state energy balance are described in this section. The steady-state segregated solver is used in this work, which results in the governing equations being solved sequentially.

FLUENT uses a control-volume method to solve the governing equations. The equations are discretized for each computational cell. In using this solution method, the CFD model stores flow properties (e.g., dependent variables) at the cell centers. Face values are required for the convection terms in the discretized equations. Face values are obtained by interpolation from the cell centers using a second-order upwind scheme for the momentum and energy equations and a first-order upwind scheme for the turbulence equations. It is noted that the diffusion terms in the equations are central-differenced and are formally second-order accurate.

Because the equation set being solved is linearized, it is necessary to control the rate of change of the flow/energy variables at each iteration step. Under-relaxation parameters are assigned to pressure, momentum, energy, turbulence kinetic energy, turbulence dissipation rate, and a variety of others that go unmodified from default settings (usually 1.0). For the buoyancy driven flow problems considered in this report, the default settings for the under-relaxation parameters for the flow equations are too high. Therefore, additional under-relaxation is necessary to obtain a converged solution. For the lower Rayleigh number cases ($<10^8$), the under-relaxation parameters for the flow equations are specified at about 0.1 or so (turbulence dissipation rate is set slightly lower). Typically, the under-relaxation for the energy equation is maintained at 1.0. For the higher Rayleigh number cases ($>10^8$), the under-relaxation parameters for the flow equations are specified slightly smaller than 0.1. For some of the cases above about 10^9, under-relaxation parameters may be set as low as 0.05.

For simulations using a scaled gravity vector (refer to Table 5 for the cases), the lowest Rayleigh number flow solution is given a reasonable uniform initial starting point for fluid velocity, temperature, and turbulence quantities. Additional iterations are required for solution convergence. Most of the flow solutions for increasing Rayleigh numbers are achieved by starting from a previously converged solution at a lower Rayleigh number. For instance, a flow solution at a Rayleigh number of $7x10^7$ is started from a converged flow solution at a Rayleigh of $7x10^6$. However, in some of the large Rayleigh number cases ($>10^9$), final convergence required a uniform initial starting point rather than that obtained from using a previously converged solution at a lower Rayleigh number when it was observed that the equation residuals could not be substantially reduced and heat transfer convergence was not achieved (e.g., heat transfer rate was too low). This nuance reflects the non-linearity of the equation set being solved. For simulations without gravity scaling (for example, from Table 5 for a full-scale simulation with a temperature difference of 50°C), the flow solution is given a uniform initial starting point for fluid velocity, temperature, and turbulence quantities.
A flow solution is considered to have converged after all equation residuals have been reduced by about 4 to 5 orders of magnitude. For the higher Rayleigh number flow cases, this may require about 10,000 or more iterations to achieve. A final convergence criteria specified in the CFD simulations is

based on an overall steady-state energy balance. When the energy imbalance between cylinders is at or below about 1-4%, the flow simulation is assumed to be at steady state. Therefore, when the residuals are reduced by 4 to 5 orders of magnitude and the energy imbalance is about 4% or less, the flow simulation is complete.

2.7 Results of the Comparative Heat Transfer Study: Average Equivalent Thermal Conductivity

This section details the development of an average equivalent thermal conductivity for natural convection heat transfer, k_{eq}. An equivalent thermal conductivity attempts to model natural convection heat transfer by specifying an enhanced thermal conductivity for use in a conduction-only model. However, fluid velocities cannot be computed using this approach. Figure 4 illustrates the average equivalent thermal conductivity from the two-dimensional CFD simulation results (without a drip shield) with a temperature difference of 20°C. The figure also includes horizontal concentric cylinder results at the same geometric scale as the YMP geometries (Francis et al., 2002). Finally, it contains the results of a full-scale eccentric inner cylinder without a flow blockage (no invert floor or drip shield) in order to separately evaluate the effect of the floor. In addition to simulation results, Figure 4 contains heat transfer correlation equations from the literature. The solid and dashed lines are from Kuehn and Goldstein (1976b, 1978) for horizontal concentric cylinders evaluated at the scale of YMP. The figure illustrates the average equivalent thermal conductivity

$$k_{eq} = \frac{Q}{Q_{cond}} \tag{4}$$

as a function of the characteristic gap-width Rayleigh number. In the average equivalent thermal conductivity definition, Q is the total heat transfer rate from a given surface while Q_{cond} is a conduction-only heat transfer rate from the same surface. The total heat transfer rate at steady state is computed as the following:

$$Q \approx \int_{A_i} q_i dA_i \approx -\int_{A_o} q_o dA_o \tag{5}$$

where the integral in equation (5) is evaluated using the CFD model. The conduction heat transfer rate at steady state is computed similarly as

$$Q_{cond} \approx \int_{A_i} q_{cond_i} dA_i \approx -\int_{A_o} q_{cond_o} dA_o \tag{6}$$

where the integral in equation (6) is also evaluated using the CFD model. All three geometric scales (25%, 44%, and full-scale) investigated by YMP are presented in the figure.

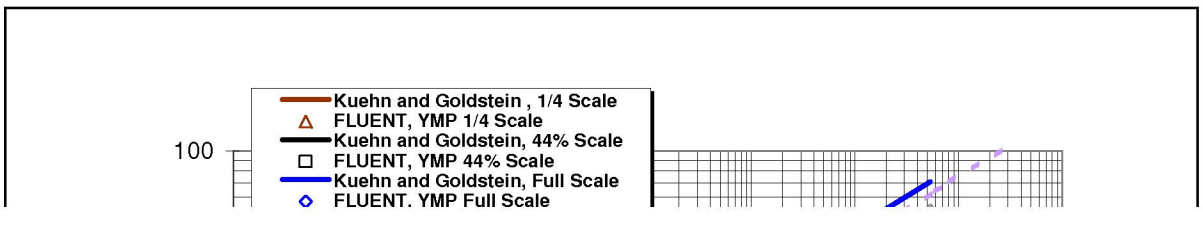

Figure 4 illustrates that the equivalent thermal conductivity for the YMP geometry with eccentricity and invert floor is considerably less than the existing heat transfer correlations for concentric cylinders. Although the actual natural convection heat transfer rate is greater for the YMP geometry (when compared to concentric cylinder cases), the pure conduction heat transfer rate in the eccentric annulus with invert is larger still and overcomes the increase in natural convection (e.g., for full-scale horizontal concentric cylinders, $Ra_L = 5.3x10^9$: $Q = 85$W and $Q_{cond} = 1.7$W; for full-scale YMP, $Ra_{Lc} = 4.11x10^9$: $Q = 89$W and $Q_{cond} = 2.9$W). Therefore, the ratio of natural convection to pure conduction (e.g., k_{eq}) is smaller than in the simple geometries (concentric and eccentric without invert). The existing natural convection heat transfer correlation equations shown in Figure 4 were developed for concentric and/or eccentric cylindrical annuli. It is noted that the equivalent thermal conductivities for YMP geometries are lower. Therefore, based on the CFD simulation results of the YMP geometries shown in Figure 4, it is clear that a heat transfer correlation equation more suited to a complex geometry including eccentricity with a flow blockage (invert) is required.

Likewise, Figure 5 shows the two-dimensional CFD numerical simulation results for geometries including a drip shield with an overall temperature difference of 20°C. Heat transfer results inside and outside the drip shield are illustrated as a function characteristic gap-width Rayleigh number. An example of the heat transfer rates inside and outside the drip shield are given for Rayleigh numbers of $4.54x10^7$ and $1.32x10^9$. Inside the drip shield the convection heat transfer rate is $Q = 33$W and the

conduction heat transfer rate is $Q_{cond} = 2.5$W. Outside the drip shield the convection heat transfer rate is Q = 39W and the conduction heat transfer rate is $Q_{cond} = 1.6$W. Similar to the geometry without a drip shield, the ratio of natural convection to pure conduction (e.g., k_{eq}) is smaller than in the simple geometries (concentric and eccentric without invert). All three geometric scales (25%, 44%, and full-scale) important to YMP are presented in this figure. As before, Figure 5 indicates that the Kuehn and Goldstein correlation equations overestimate the effective heat transfer rates for natural convection both inside and outside the drip shield.

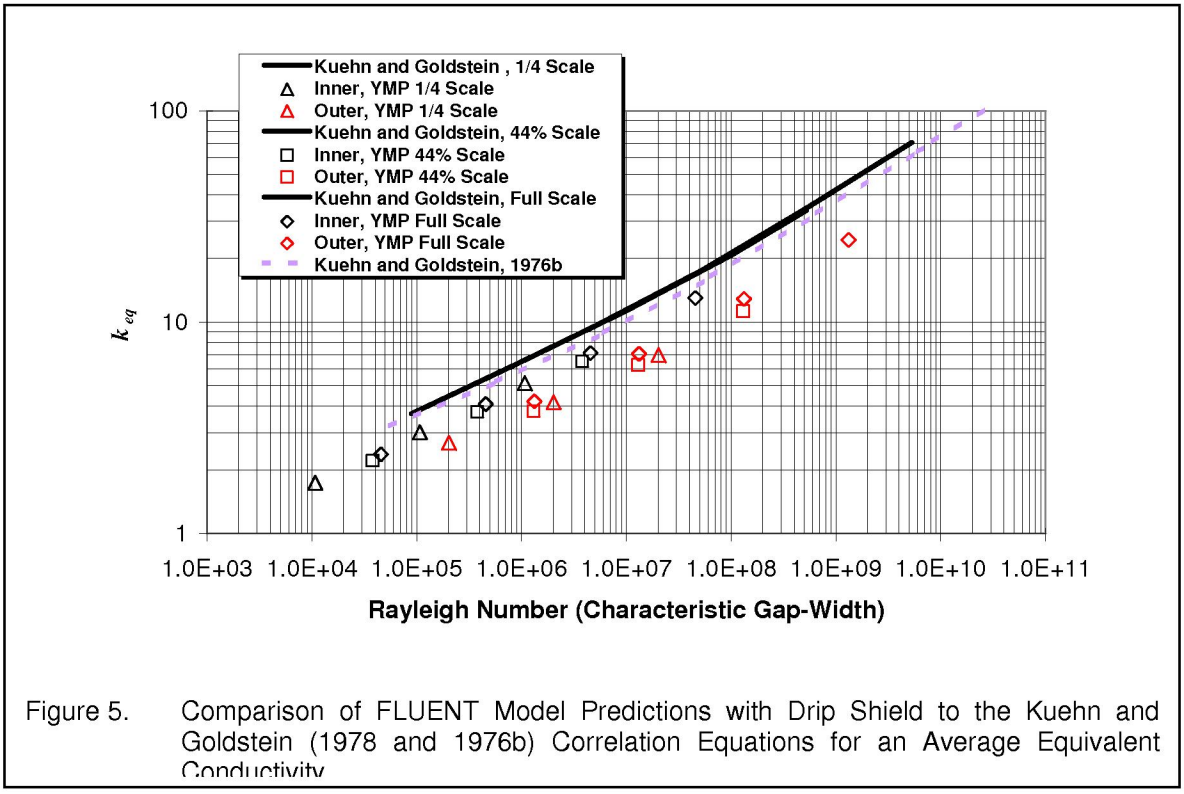

Figure 5. Comparison of FLUENT Model Predictions with Drip Shield to the Kuehn and Goldstein (1978 and 1976b) Correlation Equations for an Average Equivalent Conductivity

It is evident from Figures 4 and 5 that the YMP geometries are not well represented by the standard literature correlations for natural convection heat transfer. This is an important point as it indicates the effect that enclosure geometry imposes on the overall heat transfer rates. Use of correlation equations for natural convection from the literature overestimates the natural convection heat transfer rates from the waste packages in the YMP drifts. Figures 4 and 5 illustrate the average equivalent thermal conductivities for the 25%, 44%, and full-scale average inner diameter geometries. It is noted from the figure that the scaled (25% and 44%) YMP geometries essentially fall on the same line as the full-scale YMP results. Figures 6 – 8 illustrate only the full-scale results including the small, average, and large inner cylinder diameters. Therefore, the development of YMP-specific heat transfer correlations equations is based on Figures 6 – 8 for full-scale results only.

2.7.1 Correlation of Results

2.7.1.1 Without Drip Shield

Heat transfer correlation equations specifically designed for YMP geometries can be derived by curve fitting the CFD model predictions shown in Figures 4 and 5. Figure 6 illustrates a curve fit for the average diameter full-scale data shown in Figure 4 for 20°C and the additional full-scale model data resulting from the 5, 20, and 50°C temperature differences. A simple linear fit on a log-log plot is used to generate a YMP-specific correlation equation for natural convection heat transfer without a drip shield.

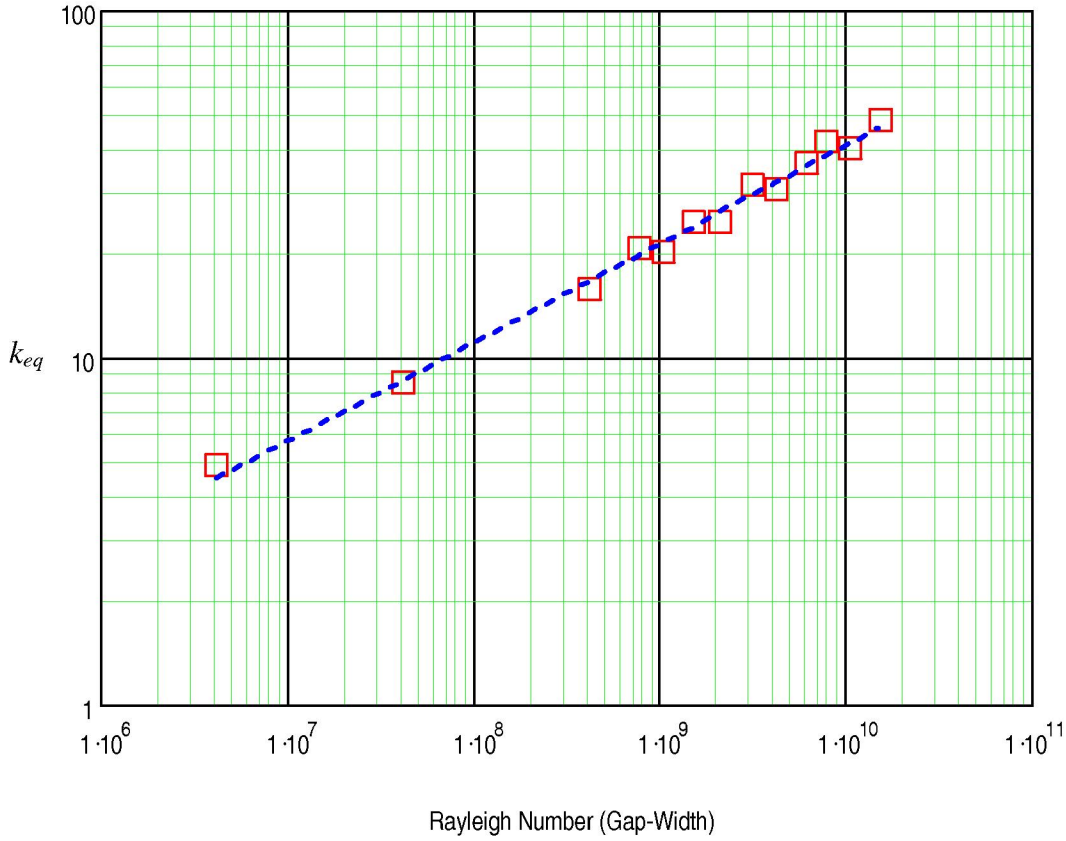

Figure 6. Development of a YMP Specific Heat Transfer Correlation Equation for Full-Scale without Drip Shield.

The resulting heat transfer correlation equation is written in terms of the temperature difference across the enclosure and the characteristic gap-width defined by equation (2). The average equivalent thermal conductivity without a drip shield is the following:

$$k_{eq} = 0.060\left[\frac{g\beta\Delta T L_c^3}{\nu\alpha}\right]^{0.284}$$
$$\approx 2.23x10^4\,\overline{T}^{-1.335}\Delta T^{0.284} L_c^{0.852} \quad (7)$$

and,

$$k_{eff,th} = k_{eq} * k_a(\overline{T})$$

where ΔT is in (°C or K because it is a temperature difference) and L_c is in meters. The average equivalent thermal conductivity (k_{eq}) is a *dimensionless* quantity. The effective thermal conductivity ($k_{eff,th}$) includes the effects of natural convection heat transfer and has units of W/m-K. It is written in terms of the stagnant air thermal conductivity, which is a function of the average fluid temperature. The coefficient of determination for the correlation equation is $r^2 = 0.985$. An r^2 of one indicates a perfect fit. The curve fit in equation (7) is reasonably close to one, thus indicating a good fit. The constraints for the YMP-specific correlation equation for natural convection heat transfer are the following:

1. the fluid Prandtl number is Pr ≅ 0.7 (Note: when using the second form of the equation, the working fluid is air)
2. the applicable temperature difference range is 0.02°C ≤ ΔT ≤ 50°C
3. thermal properties evaluated at an average fluid temperature (Note: when using the second form of the equation, $\overline{T}$ is the average fluid temperature in absolute temperature, K)
4. the applicable characteristic gap-width range is 1.58m ≤ L_c ≤ 2m
5. no drip shield

Equation (7) should be applied within the above constraints when evaluating the average equivalent thermal conductivity for full-scale YMP geometries (eccentric placement with an invert).

2.7.1.2 With Drip Shield

A similar correlating analysis is performed for the full-scale cases with a drip shield. Heat transfer correlation equations are derived for flow conditions both inside and outside the drip shield. Consider first a correlation derived for conditions inside the drip shield. Figure 7 illustrates a curve fit for the average diameter full-scale data shown in Figure 5 for 20°C and the additional full-scale model data resulting from the 5, 20, and 50°C temperature differences. A simple linear fit on a log-log plot is used to generate a YMP-specific correlation equation for natural convection heat transfer inside the drip shield.

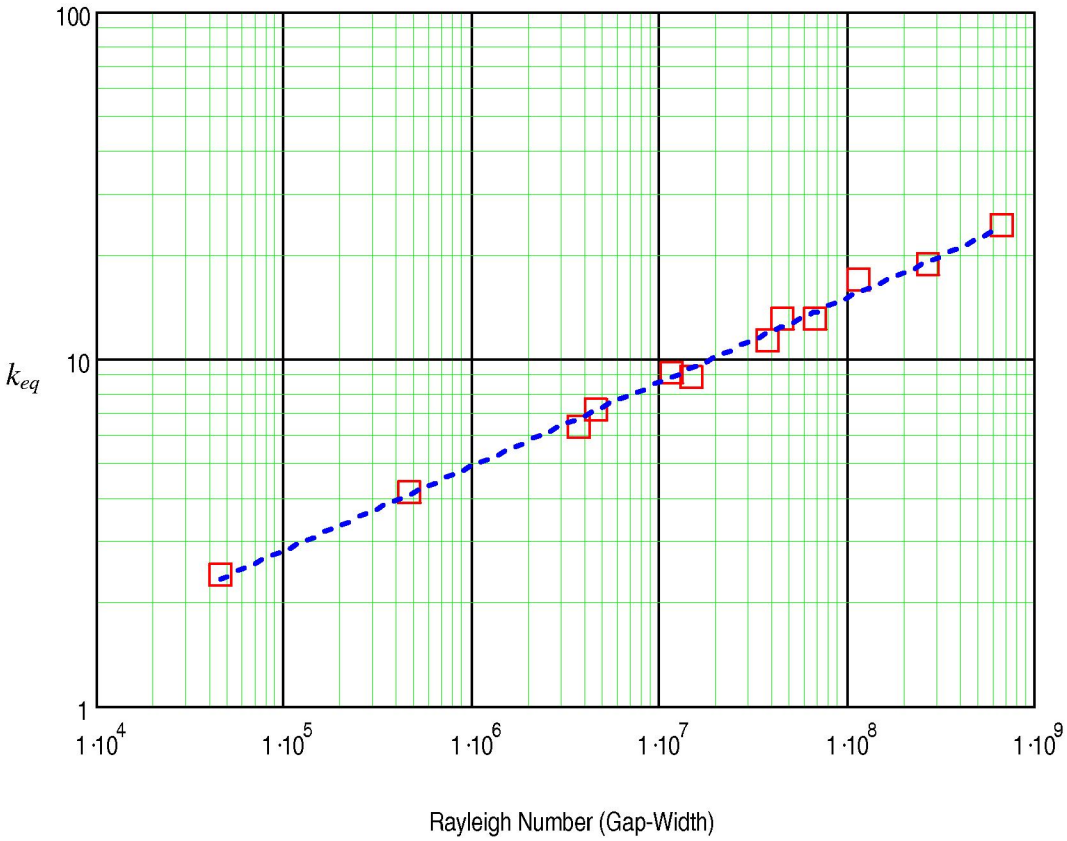

Figure 7. Development of a YMP Specific Heat Transfer Correlation Equation for Full-Scale with Drip Shield (Inside Drip Shield).

As in the previous section, the correlation equation is written in terms of the temperature difference across the enclosure inside the drip shield and the characteristic gap-width defined by equation (2). The average equivalent thermal conductivity is the following:

$$k_{eq} = 0.171\left[\frac{g\beta\Delta T L_c^3}{\nu\alpha}\right]^{0.243} \approx 10^4 \overline{T}^{-1.142}\,\Delta T^{0.243} L_c^{0.729} \tag{8}$$

and,

$$k_{eff,th} = k_{eq} * k_a(\overline{T})$$

where ΔT is in (^{o}C or K because it is a temperature difference) and L_c is in meters. The average equivalent thermal conductivity (k_{eq}) is a *dimensionless* quantity. The effective thermal conductivity

($k_{eff,th}$) includes the effects of natural convection heat transfer and has units of W/m-K. It is written in terms of the stagnant air thermal conductivity, which is a function of the average fluid temperature. The coefficient of determination for this correlation equation is $r^2 = 0.992$. The curve fit in equation (8) is reasonably close to one. The constraints for the YMP-specific correlation equation for natural convection heat transfer are the following:

1. the fluid Prandtl number is Pr ≅ 0.7 (Note: when using the second form of the equation, the working fluid is air)
2. the applicable temperature difference range is $0.0108^{\circ}C \leq \Delta T \leq 27^{\circ}C$
3. thermal properties evaluated at an average fluid temperature (Note: when using the second form of the equation, $\overline{T}$ is the average fluid temperature in absolute temperature, K)
4. the applicable characteristic length range is $0.3m \leq L_c \leq 0.9m$
5. inside the drip shield

Equation (8) should be applied within the above constraints when evaluating the equivalent thermal conductivity for full-scale YMP geometries inside the drip shield (eccentric placement with invert and drip shield).

A similar correlation equation is obtained for the equivalent thermal conductivity outside the drip shield. Figure 8 illustrates a curve fit for the average diameter full-scale data shown in Figure 5 for 20°C and the additional full-scale model data resulting from the 5, 20, and 50°C temperature differences. A simple linear fit on a log-log plot is used to generate a YMP-specific correlation equation for natural convection heat transfer outside the drip shield.

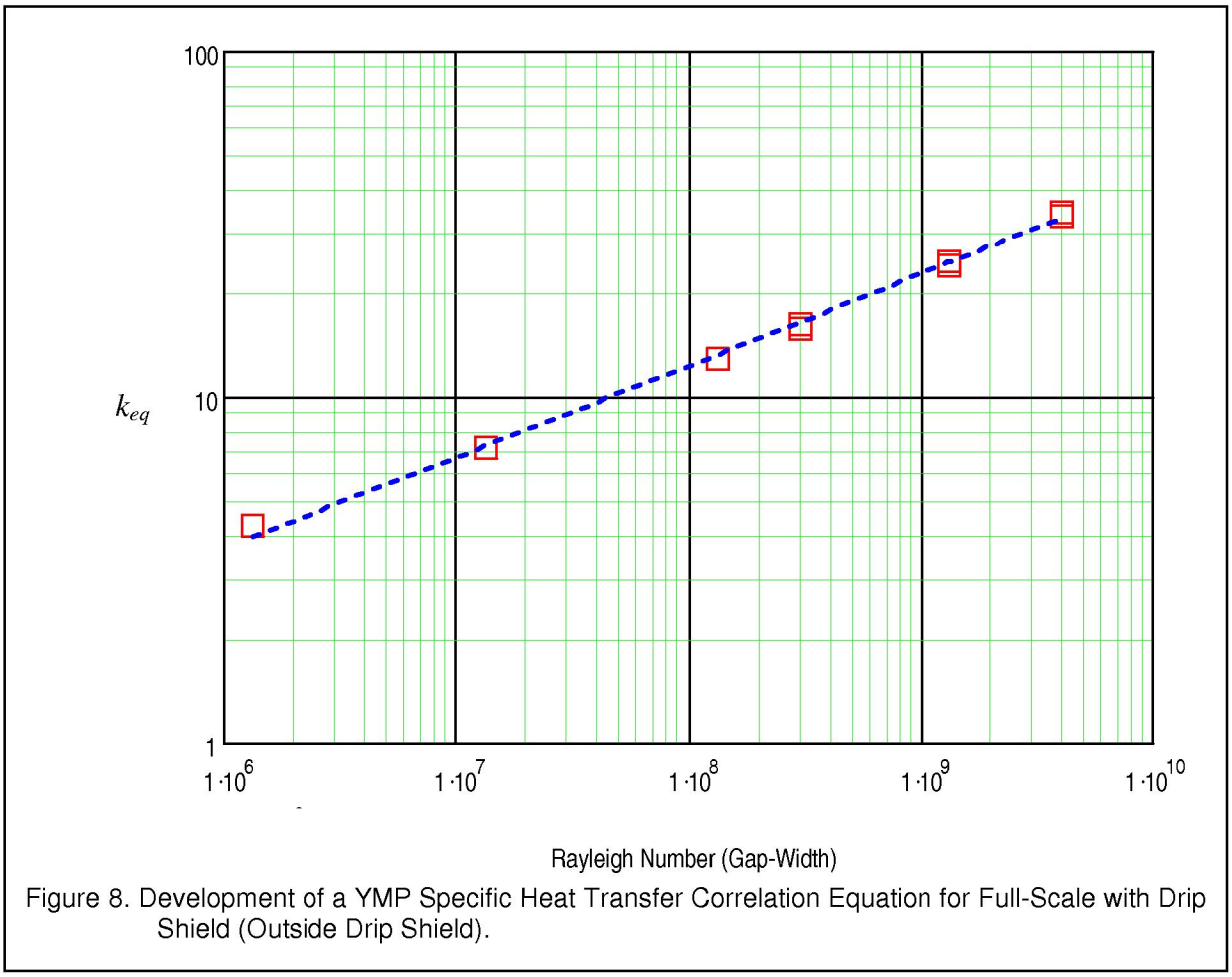

Figure 8. Development of a YMP Specific Heat Transfer Correlation Equation for Full-Scale with Drip Shield (Outside Drip Shield).

The correlation equation is written in terms of the temperature difference across the enclosure outside the drip shield and the characteristic gap-width defined by equation (2). The average equivalent thermal conductivity is the following:

$$k_{eq} = 0.097\left[\frac{g\beta\Delta T L_c^3}{\nu\alpha}\right]^{0.263} \approx 1.40x10^{4}\,\overline{T}^{-1.236}\,\Delta T^{0.263} L_c^{0.789} \tag{9}$$

and,

$$k_{eff,th} = k_{eq} * k_a(\overline{T})$$

where ΔT is in (^{o}C or K because it is a temperature difference) and L_c is in meters. The average equivalent thermal conductivity (k_{eq}) is a *dimensionless* quantity. The effective thermal conductivity

($k_{eff,th}$) includes the effects of natural convection heat transfer and has units of W/m-K. It is written in terms of the stagnant air thermal conductivity, which is a function of the average fluid temperature. The coefficient of determination for this correlation equation is $r^2 = 0.995$. The curve fit in equation (9) is reasonably close to one. The constraints for the YMP-specific correlation equation for natural convection heat transfer are:

1. the fluid Prandtl number is Pr ≅ 0.7 (Note: when using the second form of the equation, the working fluid is air)
2. the applicable temperature difference range is $0.0092^{\circ}C \leq \Delta T \leq 23^{\circ}C$
3. thermal properties evaluated at an average fluid temperature (Note: when using the second form of the equation, $\overline{T}$ is the average fluid temperature in absolute temperature, K)
4. the applicable characteristic length (L_c) is 1.5m (the characteristic length is constant because the drip shield geometry was not changed)
5. outside drip shield

Equation (9) should be applied within the above constraints when evaluating the equivalent thermal conductivity for full-scale YMP geometries outside the drip shield (eccentric placement with invert and drip shield). Table 6 summarizes each of the natural convection heat transfer correlation equations developed for full-scale YMP geometries. Table 6 also includes the Rayleigh number versions of equations (7) through (9). Figure 9 illustrates the Kuehn and Goldstein correlation equations for natural convection heat transfer together with equations (7) – (9).

Table 6. YMP Correlation Equations for Natural Convection Heat Transfer in Enclosures[1]

Case	Correlation Equation	Comments	Eq.
Full-Scale Without Drip Shield	$k_{eq} = 2.23x10^{4}\,\overline{T}^{-1.335}\,\Delta T^{0.284}\,L_c^{0.852}$ $k_{eq} = 0.060\,Ra_{L_c}^{0.284}$	$0.02^{\circ}\text{C} \le \Delta T \le 50^{\circ}\text{C}$, $1.6\text{m} \le L_c \le 2\text{m}$, $\overline{T}$ is the average fluid temperature in K $4.11x10^{6} \le Ra_{L_c} \le 1.5x10^{10}$	7
Full-Scale With Drip Shield (Inside Drip Shield)	$k_{eq} = 10^{4}\,\overline{T}^{-1.142}\,\Delta T^{0.243}\,L_c^{0.729}$ $k_{eq} = 0.171\,Ra_{L_c}^{0.243}$	$0.0108^{\circ}\text{C} \le \Delta T \le 27^{\circ}\text{C}$, $0.3\text{m} \le L_c \le 0.9\text{m}$, $\overline{T}$ is the average fluid temperature in K $4.54x10^{4} \le Ra_{L_c} \le 6.69x10^{8}$	8
Full-Scale With Drip Shield (Outside Drip Shield)	$k_{eq} = 1.4x10^{4}\,\overline{T}^{-1.236}\,\Delta T^{0.263}\,L_c^{0.789}$ $k_{eq} = 0.097\,Ra_{L_c}^{0.263}$	$0.0092^{\circ}\text{C} \le \Delta T \le 23^{\circ}\text{C}$, $L_c = 1.5\text{m}$, $\overline{T}$ is the average fluid temperature in K $1.32x10^{6} \le Ra_{L_c} \le 4.05x10^{9}$	9

1 - $k_{eff,th} = k_{eq} * k_a(\overline{T})$

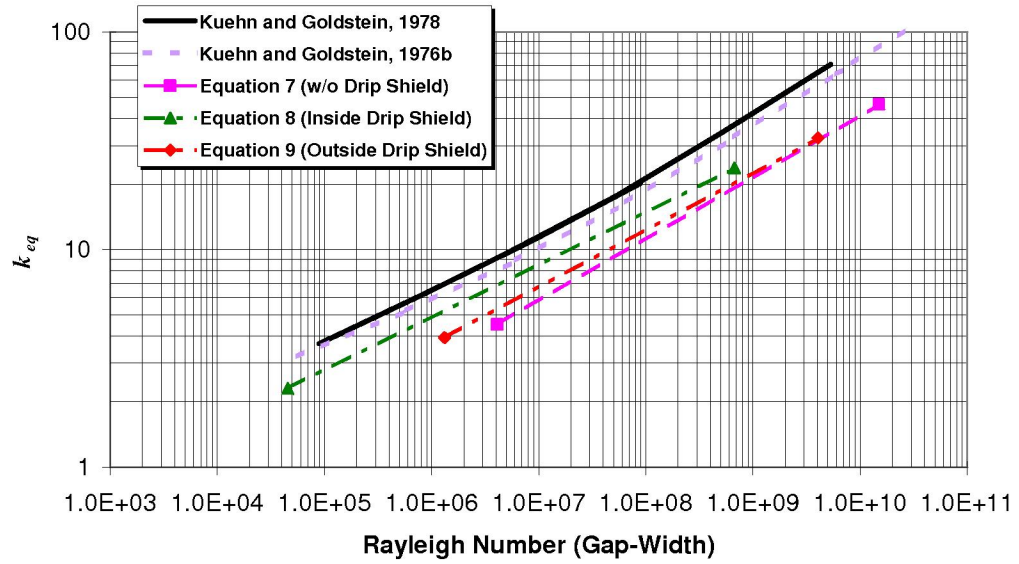

Figure 9. Comparison of Natural Convection Correlation Equations.

It is evident that the geometry associated with the YMP annulus influences the average equivalent thermal conductivity. The heat transfer correlation equations developed in the literature are specifically for the annulus formed by horizontal concentric cylinders. In some instances allowances are made for eccentric placement of the inner cylinder. However, these expressions do not account for changes in heat transfer due to flow blockages (e.g., invert, drip shield). It is clear that the YMP geometry with invert and drip shield is not adequately represented by literature correlation equations developed for an annulus formed by horizontal concentric cylinders.

2.8 Results of the Comparative Heat Transfer Study: Local Equivalent Thermal Conductivity

The figures and correlation equations developed in Section 2.7 are for an average equivalent thermal conductivity. It was shown in that section that the heat transfer correlation equations in the literature do not accurately represent the YMP geometries under consideration. Therefore, equations (7) through (9) should be applied to YMP-specific geometries when performing in-drift heat transfer analyses. It is instructive to look at how the local equivalent thermal conductivity varies around enclosure boundaries. The local variability in the system may be important when considering the distribution of temperature within an enclosure. The following figures illustrate a local equivalent thermal conductivity for natural convection heat transfer. All surfaces forming an enclosure are considered. Local effects are illustrated at angular locations around the enclosure by displaying variability in heat transfer on both the hot and the cold surfaces. Refer to Figure 10 for specific angular locations.

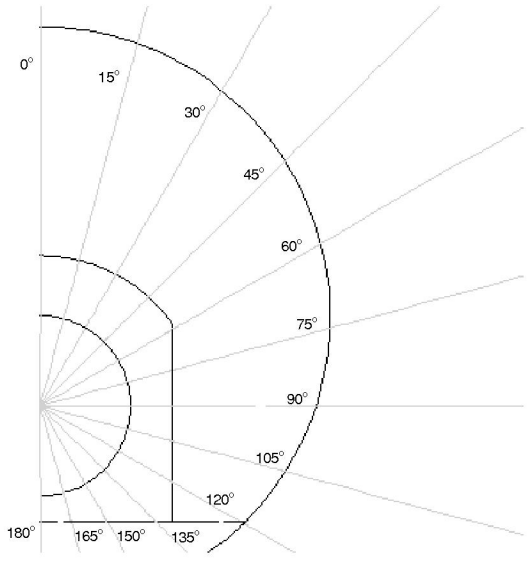

Figure 10. Locations of Local Heat Transfer Results.

The local equivalent thermal conductivity for natural convection is computed in a manner similar to equation (4). However, the equation is written in terms of individual heat transfer components on a given surface.

$$k_{eq_j} = \frac{q_j}{q_{cond_j}} \tag{10}$$

where j is equal to a specific position (e.g., $\theta = 60^{o}$) along a hot or cold bounding surface (refer to Figures 2, 3, and 10). Using equation (10), local equivalent thermal conductivities are computed for both the with and without drip shield cases. The with drip shield case contains both inside and outside surfaces inside and outside the drip shield. Figures 11, 14, and 17 illustrate local distributions of equivalent thermal conductivity at Rayleigh numbers of $4.11x10^{9}$, $4.54x10^{7}$, and $1.32x10^{9}$ for without drip shield, with drip shield (inside), and with drip shield (outside), respectively. Also included in the figures are the average equivalent thermal conductivities constituting equations (7) through (9). Figures 12, 15, and 18 illustrate the local heat fluxes for the inner surfaces normalized using an average heat flux on the inner surface. Additionally, the figures also include the conduction heat flux times the average equivalent thermal conductivity, also normalized with respect to the average heat flux. These figures illustrate the actual variability obtained from a CFD calculation and how it compares to the variability one forces when applying an effective thermal conductivity to approximate heat transfer by natural convection. Figures 13, 16, and 19 illustrate the local heat fluxes for the outer surfaces normalized using an average heat flux on the outer surface. They also include the conduction heat flux times the average equivalent thermal conductivity, also normalized with respect to the average heat flux.

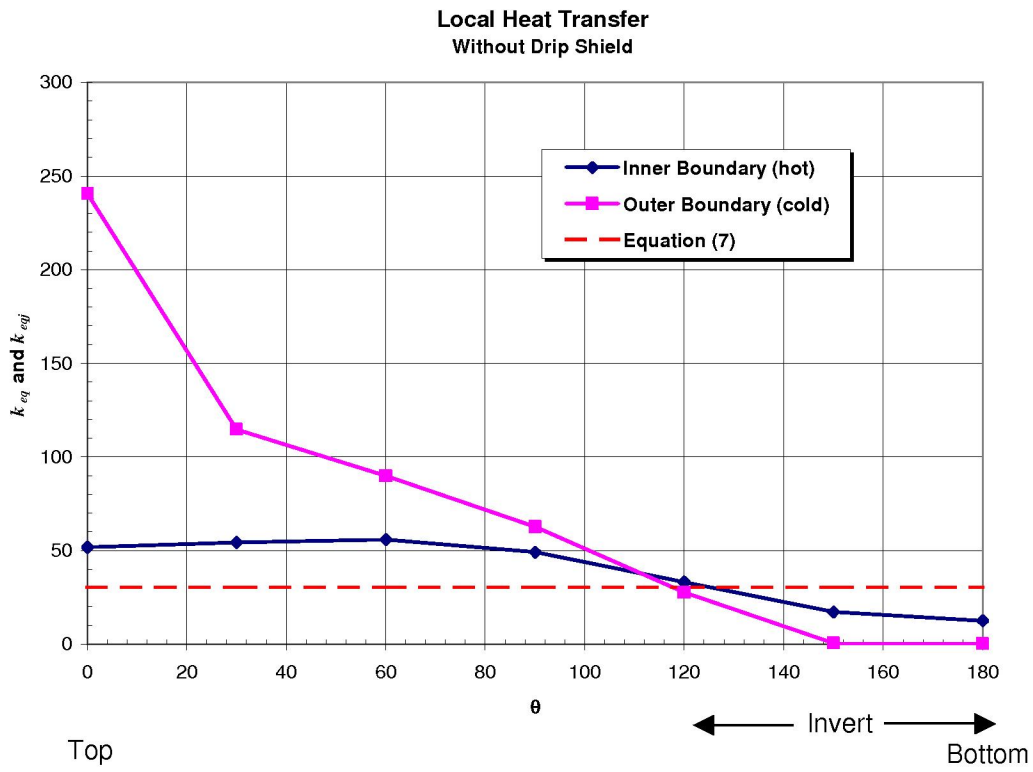

Figure 11. Local Equivalent Thermal Conductivity Without Drip Shield.

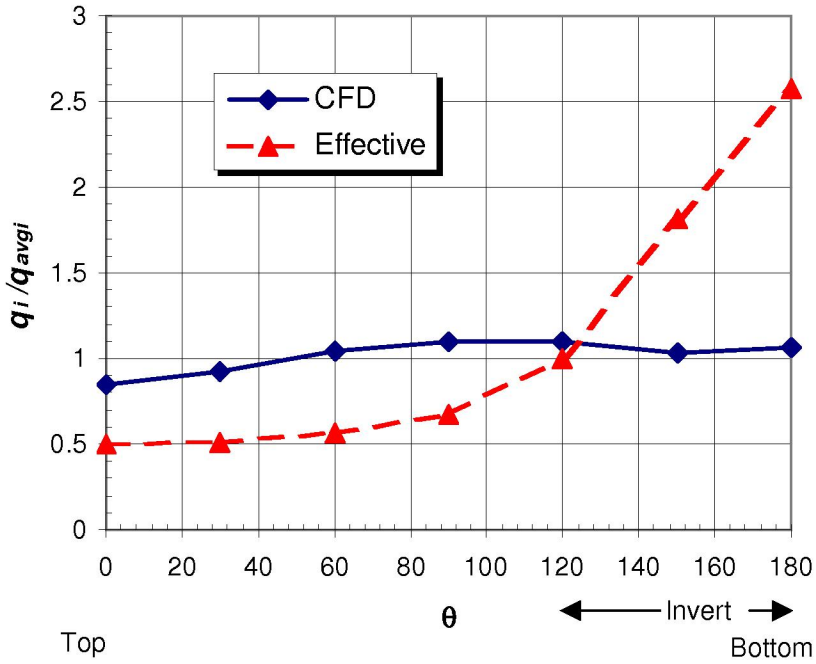

Figure 12. Local Convection on the Inner Surface using CFD and an Effective Thermal Conductivity Representation (Without Drip Shield).

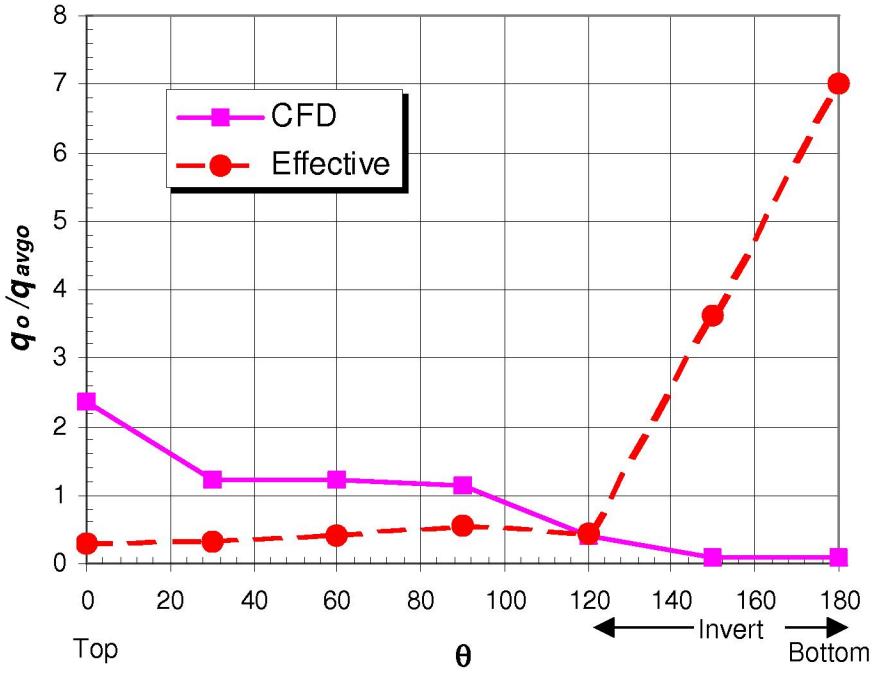

Figure 13. Local Convection on the Outer Surface using CFD and an Effective Thermal Conductivity Representation (Without Drip Shield).

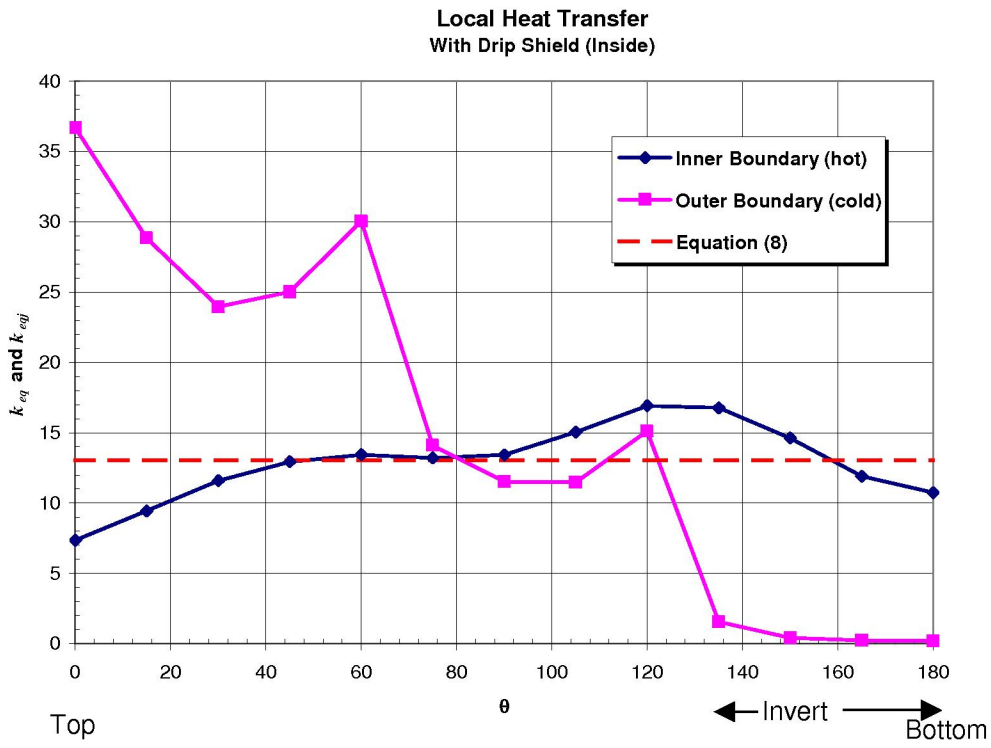

Figure 14. Local Equivalent Thermal Conductivity With Drip Shield (Inside).

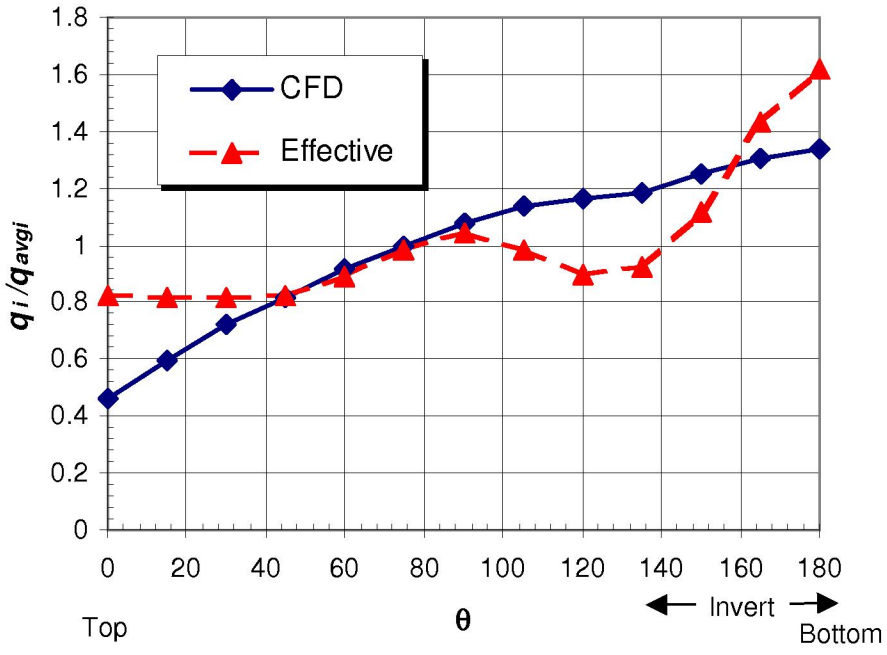

Figure 15. Local Convection on the Inner Surface using CFD and an Effective Thermal Conductivity Representation (Inside Drip Shield).

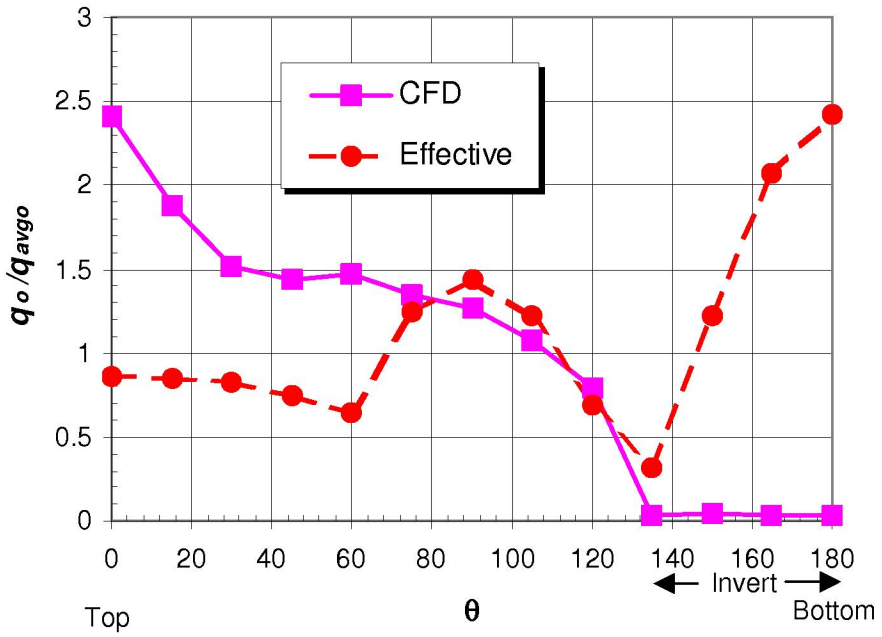

Figure 16. Local Convection on the Outer Surface using CFD and an Effective Thermal Conductivity Representation (Inside Drip Shield).

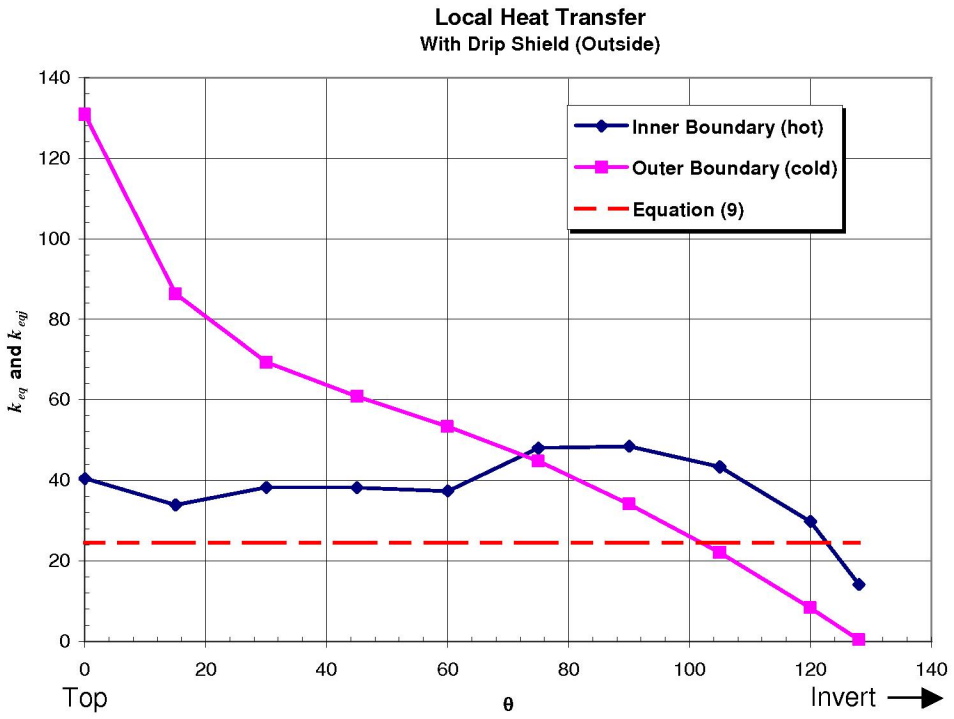

Figure 17. Local Equivalent Thermal Conductivity With Drip Shield (Outside).

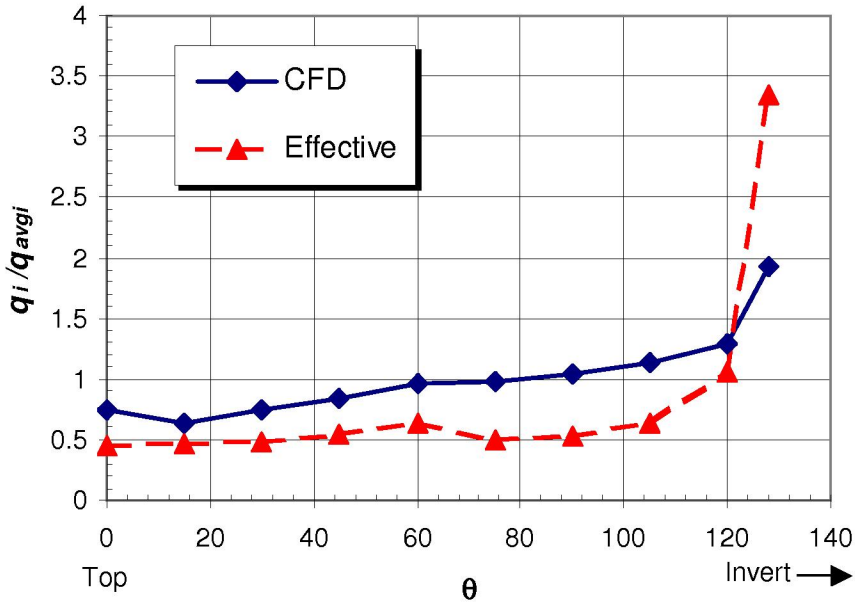

Figure 18. Local Convection on the Inner Surface using CFD and an Effective Thermal Conductivity Representation (Outside Drip Shield).

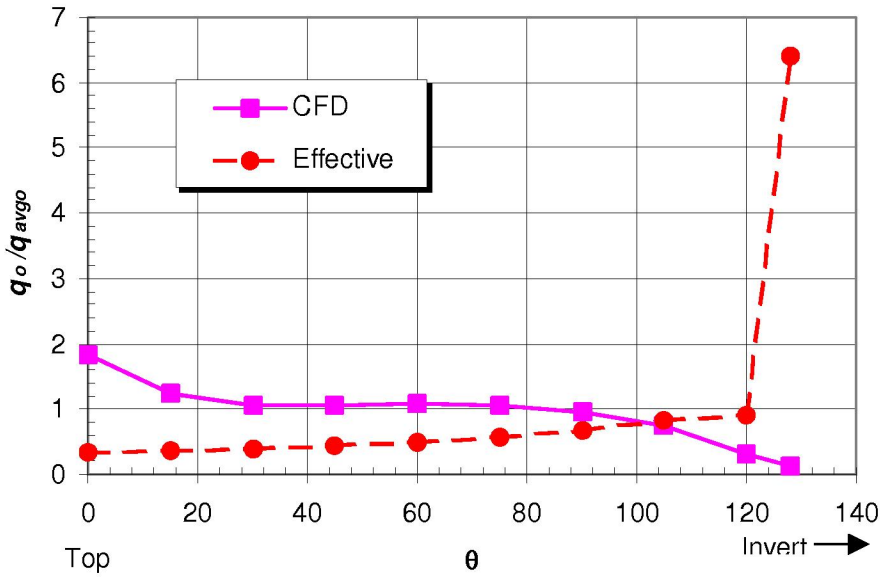

Figure 19. Local Convection on the Outer Surface using CFD and an Effective Thermal Conductivity Representation (Outside Drip Shield).

Figures 11 – 19 indicate extensive heat flux variability around the surfaces of the YMP enclosures. The convection heat flux generally increases from top to bottom on the inner surface and decreases from top to bottom on the outer surface. The conduction heat flux increases as the distance between surfaces of the enclosure decreases. The overall (integral) heat transfer rates on the inner and outer surfaces of an enclosure are identical (refer to equation (5)). For example, the overall natural convection heat transfer rate for the enclosure formed inside the drip shield is

$$Q = \int_{A_i} q_i dA_i = -\int_{A_o} q_o dA_o = 33W$$

The average equivalent thermal conductivities given by equations (7) – (9) typically underestimate the local heat transfer around the bounding surfaces of the YMP enclosures. This is because the average equivalent thermal conductivity is influenced by the increase in the conduction heat flux (refer to equation (6)). Unlike in horizontal concentric cylinders, the local conduction heat flux varies around the surfaces that make up the YMP enclosures. As the distance between the surfaces forming an enclosure decreases, the local conduction heat flux increases and hence the overall conduction term in the denominator of equation (4) increases, thus driving the average k_{eq} downward. This is coupled with the fact that the total heat flux only gradually increases from top to bottom for the inner cylinder (for example). Consequently, the average equivalent thermal conductivity is driven (downward) by a larger increase in the integral conduction heat transfer rate than that which occurs in the integral convection heat transfer rate.

This behavior suggests that the local equivalent thermal conductivity is dominated by convection in the upper half of the enclosure and by conduction in the lower half. Reference to Figures 11, 14, and 17 indicates this to be the case as both curves are typically above the average equivalent thermal conductivity curve in the upper portion of the annulus and below in the lower portion of the annulus. Consequently, an average equivalent thermal conductivity cannot reproduce the localized impact of convection heat transfer because it applies integral heat transfer rates in its definition. This fact is further illustrated in the heat flux plots for the inner and outer surfaces. Figures 12, 15, and 18 indicate the local heat flux components on the inner surfaces for each of the cases considered. The local heat fluxes are representative of those from a rigorous CFD calculation. Figures 13, 16, and 19 indicate the local heat flux components on the outer surfaces. In each figure, an *effective* convection heat flux is illustrated (defined as the conduction-only heat flux multiplied by the average equivalent thermal conductivity). The effective convection heat flux represents an approximation for heat transfer by natural convection. In the upper portion of the annulus, the effective heat flux typically underestimates the actual local convection heat flux. In the lower portion of the annulus it overestimates the local convection heat flux. In regions where the local and average equivalent thermal conductivities happen to be equal, the local and equivalent heat fluxes are equal.

Therefore, when the assumption is made that natural convection heat transfer can be approximated through the use of an average equivalent thermal conductivity, it is evident that the actual variability associated with convection heat transfer cannot be duplicated by a single equivalent parameter. Subsequently, the limitation of this assumption and its impacts on the distribution of temperature must be considered when using this simplification.

2.9 Grid Independence Study

A grid independence study is performed for the highest Rayleigh number CFD simulation without a drip shield, $1.5x10^{10}$. This numerical simulation is selected because it has the largest velocities. Vertical fluid velocity, temperature, and overall heat transfer rates are compared for two different computational grids. The working computational grid for a Rayleigh number of $1.5x10^{10}$ contains 4697 cells in the fluid region. A refined computational grid contains 7533 cells in the fluid region. The reported overall heat transfer rate for the working grid is 234 W. The overall heat transfer rate for the refined grid is 233 W. These heat transfer rates are within a fraction of a percent of each other. Velocities and temperatures from the two grids are also compared in Figures 20-23 below. The vertical velocity is compared at the eccentric position (refer to Figure 2) and at a location across the upper portion of the annulus. Figure 20 illustrates the vertical velocity (or Y velocity) at the eccentric position in this model. Figure 21 illustrates the vertical velocity in the upper portion of the annulus.

The fluid temperature is compared at the eccentric position (refer to Figure 2) and at a location across the upper portion of the annulus. Figure 22 illustrates the fluid temperature at the eccentric position in this model. Figure 23 illustrates the fluid temperature in the upper portion of the annulus (same location as Figure 21).

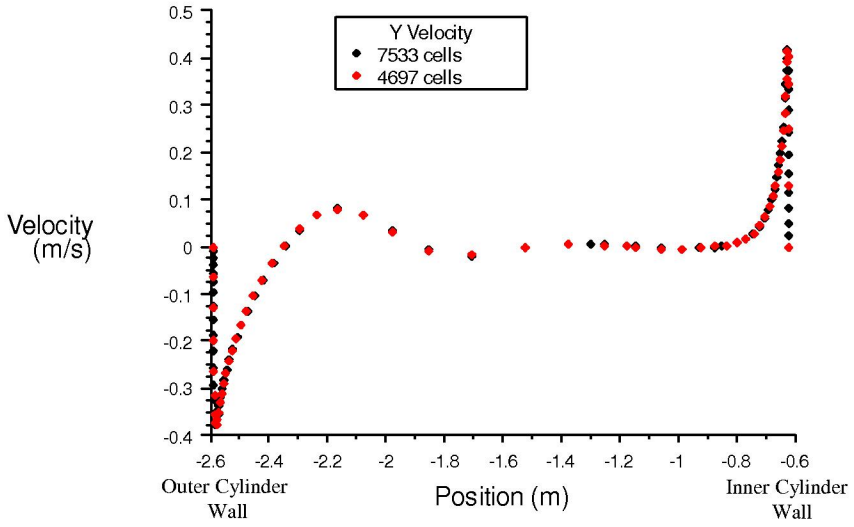

Figure 20. Vertical Velocity Profile at the Eccentric Position in the Full-Scale YMP Geometry with a Rayleigh Number of $1.5x10^{10}$.

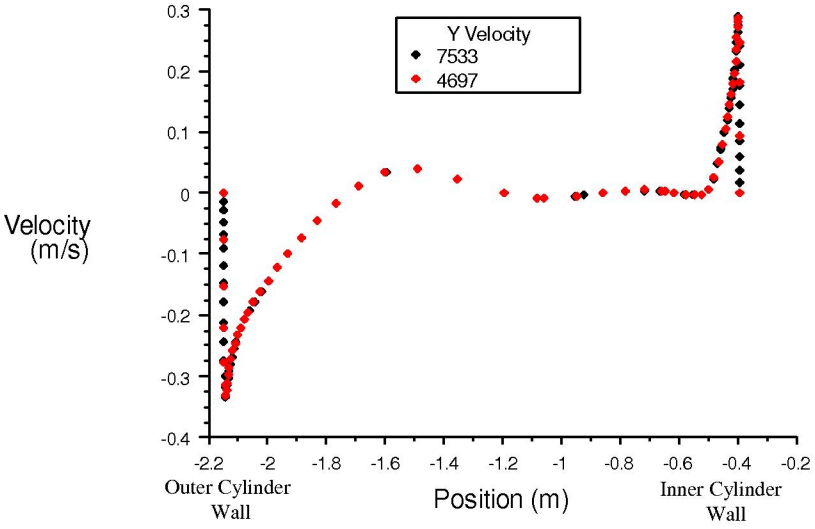

Figure 21. Vertical Velocity Profile in the Upper Annulus in the Full-Scale YMP Geometry with a Rayleigh Number of $1.5x10^{10}$.

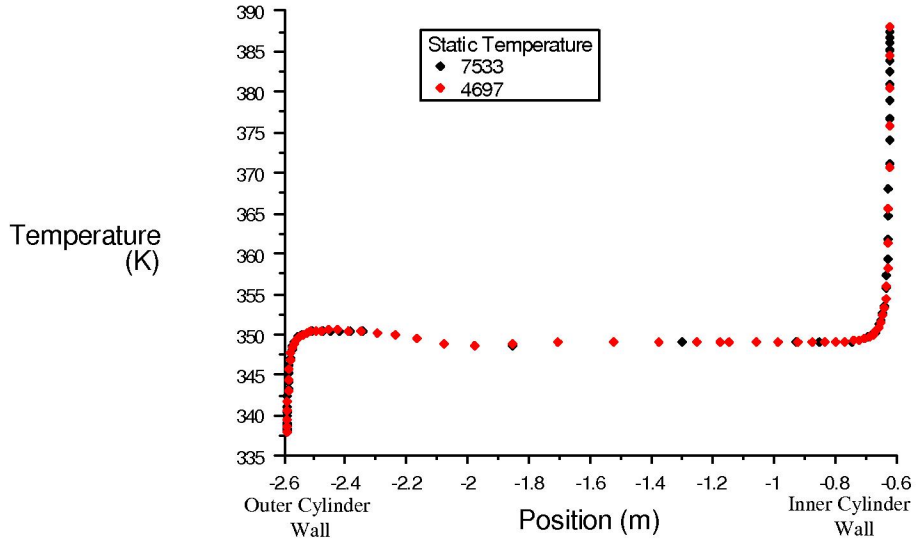

Figure 22. Temperature Profile at the Eccentric Position in the Full-Scale YMP Geometry with a Rayleigh Number of $1.5x10^{10}$.

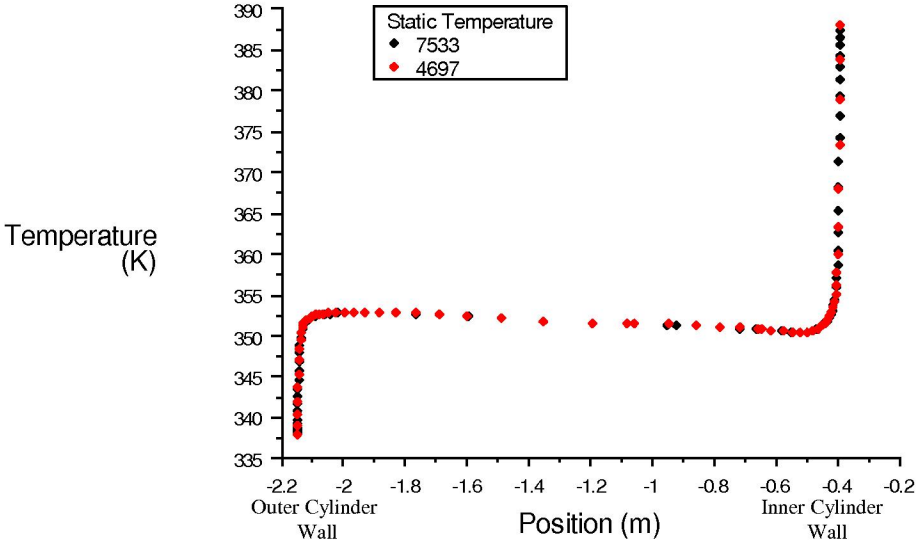

Figure 23. Temperature Profile in the Upper Annulus in the Full-Scale YMP Geometry with a Rayleigh Number of $1.5x10^{10}$.

Based on comparisons of heat transfer rate, vertical velocity, and fluid temperature, the working computational grid (4697 cells) for the full-scale model with a Rayleigh number of $1.5x10^{10}$ provides an adequate description of the physical processes occurring within the heated annulus. Because the other no drip shield CFD models at a minimum contain the same number of cells (all of which are at a lower Rayleigh number than $1.5x10^{10}$) as the working grid analyzed above, grid independence has indeed been achieved for all no drip shield cases. The drip shield CFD models contain even more computational cells (e.g., more boundary layers to resolve) at much lower Rayleigh numbers than their no drip shield counterparts. This being the case, grid independence is assumed to be achieved for all drip shield cases as well.

3 DISCUSSION

Equivalent thermal conductivity correlation equations from the literature (developed for horizontal concentric cylinders) evaluated at the scale of YMP result in larger equivalent thermal conductivities (for natural convection) than those computed from the numerical simulations specifically developed for YMP enclosures (e.g., eccentric cylinder placement with a flow blockage below the inner cylinder, with or without drip shield). This is true for Rayleigh numbers in the range of $7x10^5$ to $2x10^{10}$ for no drip shield simulations, $1x10^4$ to $7x10^8$ inside the drip shield, and $2x10^5$ to $4x10^9$ outside the drip shield, spanning both laminar and turbulent flow regimes. Therefore, application of general correlation equations obtained from the literature to YMP geometries overestimates natural convection heat transfer rates in the annulus. Subsequently, three new natural convection heat transfer correlation equations based on CFD simulation results specifically for YMP geometries have been derived in this report. These correlation equations should be used when computing natural convection heat transfer in YMP enclosures instead of the existing heat transfer correlation equations in the literature. The new correlation equations apply to without drip shield and with drip shield (both inside and outside) geometric configurations for the stated flow conditions. These equations are applicable over a broad range of Rayleigh numbers.

Local equivalent thermal conductivities have been plotted around the surfaces of the YMP enclosures and compared to the average equivalent thermal conductivities obtained from equations (7) – (9). It is noted that extensive localized convection heat transfer occurs in YMP enclosures that will not be captured through the use of an average equivalent thermal conductivity. This feature may have a strong affect on how heat and water vapor (and condensation) is transported within the YMP drifts both inside and outside the drip shield.

4 REFERENCES

Bejan, A. 1995. *Convection Heat Transfer.* 2nd Edition. New York, New York: John Wiley & Sons.

Bishop, E.H. 1988. "Heat Transfer by Natural Convection of Helium Between Horizontal Isothermal Concentric Cylinders at Cryogenic Temperature." *Journal of Heat Transfer, 111*, 109-115.

Bishop, E.H., Carley C.T., and Powe, R.E. 1968. "Natural Convective Oscillatory Flow in Cylindrical Annuli." *International Journal of Heat and Mass Transfer,* Vol. 11, 1741-1752. Pergamon Press.

Char, M-I. and Hsu, Y-H. 1998. "Comparative Analysis of Linear and Nonlinear Low-Reynolds Number Eddy Viscosity Models to Turbulent Natural Convection in Horizontal Cylindrical Annuli." *Numerical Heat Transfer, Part A*, (33), 191-206. Washington, DC, Taylor & Francis.

Desai, C. P. and Vafai, K. 1994. "An Investigation and Comparative Analysis of Two- and Three-Dimensional Turbulent Natural Convection in a Horizontal Annulus." *International Journal of Heat and Mass Transfer, 37*, (16), 2475-2504. New York, New York: Pergamon Press.

Farouk, B. and Guceri, S.I. 1982. "Laminar and Turbulent Natural Convection in the Annulus Between Horizontal Concentric Cylinders." *Journal of Heat Transfer, 104*, (4), 631-636. New York, New York: American Society of Mechanical Engineers.

Fluent Incorporated. 2001. Fluent 6 User's Guide. Volumes 1 to 5. Lebanon, New Hampshire: Fluent Incorporated.

Francis, N.D., Itamura, M.T., Webb, S.W., and James, D.L. 2002. "CFD Calculation of Internal Natural Convection in the Annulus between Horizontal Concentric Cylinders." SAND2002-3132, Sandia National Laboratories, Albuquerque, New Mexico.

Francis, N.D., Itamura, M.T., Webb, S.W., and James, D.L. 2003. "Two-Dimensional CFD Calculations for YMP Natural Convection Tests." SAND2003-0245, Sandia National Laboratories, Albuquerque, New Mexico.

Francis, N.D., Itamura, M.T., Webb, S.W., and James, D.L. 2003a. "In-Drift Natural Convection Sensitivity Studies for the LTOM Repository Design." 2003 International High-Level Radioactive Waste Management Conference (In Draft).

Fusegi, T. and Farouk, B. 1986. "A Three Dimensional Study of Natural Convection in the Annulus Between Horizontal Concentric Cylinders." *Heat Transfer 1986, Proceedings of The Eighth International Heat Transfer Conference.* C.L. Tien, V.P. Carey, and J.K. Ferrell. 4, 1575-1580. Hemisphere Publishing Corporation.

Gebhart, G., Jaluria, Y., Mahajan, R.L., and Sammakia, B. 1988. Buoyancy-Induced Flows and Transport. Reference Edition. New York, New York: Hemisphere Publishing Corporation.

Kuehn, T. H. 1976. *Natural Convection Heat Transfer from a Horizontal Circular Cylinder to a Surrounding Cylindrical Enclosure*. Ph.D. Dissertation. Ann Arbor, Michigan: University Microfilms International/University of Minnesota.

Kuehn, T.H. and Goldstein, R.J. 1976a. "An Experimental and Theoretical Study of Natural Convection in the Annulus Between Horizontal Concentric Cylinders." *Journal of Fluid Mechanics, 74*, (part 4), 695-719

Kuehn, T.H. and Goldstein, R.J. 1976b. "Correlating Equations for Natural Convection Heat Transfer Between Horizontal Circular Cylinders." *International Journal of Heat and Mass Transfer, 19*, (10), 1127-1134. New York, New York: Pergamon Press.

Kuehn, T.H. and Goldstein, R.J. 1978. "An Experimental Study of Natural Convection Heat Transfer in Concentric and Eccentric Horizontal Cylindrical Annuli." *Journal of Heat Transfer, Transactions of the ASME, 100*, ([4]), 635-640. [New York, New York: American Society of Mechanical Engineers].

Lis, J. 1966. "Experimental Investigation of Natural Convection Heat Transfer in Simple and Obstructed Horizontal Annuli." *Third International Heat Transfer Conference, 2*, (2), 196-204

McLeod, A.E. and Bishop, E.H. 1989. "Turbulent Natural Convection of Gases in Horizontal Cylindrical Annuli at Cryogenic Temperatures." *International Journal of Heat and Mass Transfer, 32*, (10), 1967-1978. New York, New York: Pergamon Press.

Raithby, G.D. and Hollands, K.G.T. 1975. "A General Method of Obtaining Approximate Solutions to Laminar and Turbulent Free Convection Problems." In *Advances in Heat Transfer*, 11, 265-315 of Advances in Heat Transfer. New York, New York: Academic Press.

Vafai, K., Desai, C.P., Iyer, S.V. and Dyko, M.P. 1997. "Buoyancy Induced Convection in a Narrow Open-Ended Annulus." *Journal of Heat Transfer, 119*, (3), 483-494. New York, New York: The American Society of Mechanical Engineers.

Webb, S.W., Francis, N.D., Dunn, S.D., Itamura, M.T., and James, D.L. 2002. "Thermally-Induced Natural Convection Effects in Yucca Mountain Drifts." *Journal of Contaminant Hydrology.* (In Press).

DISTRIBUTION

External

Sandra Dalvit-Dunn
Science Engineering Associates
3203 Richards Lane
Santa Fe, NM 87505

John Del Mar
Science Engineering Associates
3203 Richards Lane
Santa Fe, NM 87505

William Lowry
Science Engineering Associates
3203 Richards Lane
Santa Fe, NM 87505

Thomas A. Buscheck
Lawrence Livermore National Laboratory
7000 East Avenue
Livermore, CA 94550-9234

Lee Glascoe
Lawrence Livermore National Laboratory
7000 East Avenue
Livermore, CA 94550-9234

Eric Sonnenthal
Berkeley Lab
1 Cyclotron Rd
Berkeley, CA 94720

Michael J. Anderson
1180 Town Center Drive
Las Vegas, NV 89144

James A. Blink
1180 Town Center Drive
Las Vegas, NV 89144

Veraun Chipman
1180 Town Center Drive
Las Vegas, NV 89144

Thomas W. Doering
1180 Town Center Drive
Las Vegas, NV 89144

Harris Greenberg
MTS
P.O. Box 364629
Yucca Mountain Site Characterization Office
Las Vegas, NV 89036

Matthew D. Hinds
1180 Town Center Drive
Las Vegas, NV 89144

James Houseworth
1180 Town Center Drive
Las Vegas, NV 89144

Norman Kramer
1180 Town Center Drive
Las Vegas, NV 89144

Bruce Kirstein
1180 Town Center Drive
Las Vegas, NV 89144

Junghun Leem
1180 Town Center Drive
Las Vegas, NV 89144

Helen Marr
1180 Town Center Drive
Las Vegas, NV 89144

Delwin Mecham
1180 Town Center Drive
Las Vegas, NV 89144

Randolph Schreiner
1180 Town Center Drive
Las Vegas, NV 89144

Daniel A. Thomas
1180 Town Center Drive
Las Vegas, NV 89144

Universities

Darryl James (2)
Texas Tech University
Department of Mechanical Engineering
Box 41021
Lubbock, TX 79409-1021

Thomas H. Kuehn
Department of Mechanical Engineering
Institute of Technology
University of Minnesota
111 Church St. SE
Minneapolis, MN 55455-0111

Kambiz Vafai
University of California, Riverside
Department of Mechanical Engineering
A363 Bourns Hall
Riverside, CA 92521

Internal

MS	Org.	
0701	6100	P. B. Davies
0706	6113	R. E. Finley
0718	6141	C. Lopez
0718	6141	K. B. Sorenson
0719	6131	S. M. Howarth
0719	6131	E. Lindgren
0719	6131	S. W. Webb (10)
0735	6115	C. K. Ho
0750	6116	D. J. Borns
0751	6117	L. S. Costin
0751	6117	S. R. Sobolik
0771	6800	D. L. Berry
0776	6852	T. Hadgu
0776	6852	M. T. Itamura (5)
0776	6852	K. M. Knowles
0776	6852	E. J. Nowak
0776	6852	A. W. Reed
0778	6851	R. L. Jarek
0778	6851	C. F. Jove-Colon
0778	6851	R. J. MacKinnon
0779	6849	H. N. Jow
0779	6849	L. C. Sanchez
0821	9132	L. A. Gritzo
0826	9113	S. N. Kempka
0834	9114	J. E. Johannes
0836	9116	D. Dobranich
0836	9116	E. S. Hertel, Jr.
0836	9116	N. D. Francis (20)
0836	9117	R. O. Griffith
0836	9117	C. E. Hickox, Jr.
1399	6850	A. S. Orrell
1399	6855	C. L. Howard
0731	4415	NWM Library (2)
9018	8945-1	Central Technical Files
0899	9616	Technical Library (2)
0612	9612	Review and Approval Desk, For DOE/OSTI (1)